



# *Klebsiella pneumoniae* carbapenemase variant 44 acquires ceftazidime-avibactam resistance by altering the conformation of active-site loops

Received for publication, August 18, 2023, and in revised form, November 14, 2023 Published, Papers in Press, November 23, 2023, <https://doi.org/10.1016/j.jbc.2023.105493>

Zhizeng Sun<sup>1</sup>, Hanfeng Lin<sup>1</sup>, Liya Hu<sup>1</sup>, Neetu Neetu<sup>1</sup>, Banumathi Sankaran<sup>2</sup>, Jin Wang<sup>1</sup>, B. V. Venkataram Prasad<sup>1</sup>, and Timothy Palzkill<sup>1,\*</sup>

From the <sup>1</sup>Verna and Marrs McLean Department of Biochemistry and Molecular Pharmacology, Baylor College of Medicine, Houston, Texas, USA; <sup>2</sup>Department of Molecular Biophysics and Integrated Bioimaging, Berkeley Center for Structural Biology, Lawrence Berkeley National Laboratory, Berkeley, California, USA

Reviewed by members of the JBC Editorial Board. Edited by Chris Whitfield

*Klebsiella pneumoniae* carbapenemase 2 (KPC-2) is an important source of drug resistance as it can hydrolyze and inactivate virtually all  $\beta$ -lactam antibiotics. KPC-2 is potently inhibited by avibactam *via* formation of a reversible carbamyl linkage of the inhibitor with the catalytic serine of the enzyme. However, the use of avibactam in combination with ceftazidime (CAZ-AVI) has led to the emergence of CAZ-AVI-resistant variants of KPC-2 in clinical settings. One such variant, KPC-44, bears a 15 amino acid duplication in one of the active-site loops (270-loop). Here, we show that the KPC-44 variant exhibits higher catalytic efficiency in hydrolyzing ceftazidime, lower efficiency toward imipenem and meropenem, and a similar efficiency in hydrolyzing ampicillin, than the WT KPC-2 enzyme. In addition, the KPC-44 variant enzyme exhibits 12-fold lower AVI carbamylation efficiency than the KPC-2 enzyme. An X-ray crystal structure of KPC-44 showed that the 15 amino acid duplication results in an extended and partially disordered 270-loop and also changes the conformation of the adjacent 240-loop, which in turn has altered interactions with the active-site omega loop. Furthermore, a structure of KPC-44 with avibactam revealed that formation of the covalent complex results in further disorder in the 270-loop, suggesting that rearrangement of the 270-loop of KPC-44 facilitates AVI carbamylation. These results suggest that the duplication of 15 amino acids in the KPC-44 enzyme leads to resistance to CAZ-AVI by modulating the stability and conformation of the 270-, 240-, and omega-loops.

$\beta$ -Lactam antibiotics are the most frequently prescribed drugs for treating infections caused by various bacterial pathogens (1). These antibiotics are characterized by the four-membered  $\beta$ -lactam ring and are classified into penicillins, cephalosporins, carbapenems, and monobactams according to their chemical structures. They exhibit bactericidal effects by inhibiting the penicillin-binding protein-catalyzed transpeptidation of peptidoglycan strands of the cell wall. The

$\beta$ -lactam ring is structurally analogous to the D-Ala-D-Ala substrate, which facilitates  $\beta$ -lactam binding and covalent inhibition of penicillin-binding proteins (2). However, the extensive use of  $\beta$ -lactam antibiotics has resulted in widespread resistance to these drugs. Although multiple mechanisms exist for resistance to  $\beta$ -lactam antibiotics, the production of  $\beta$ -lactamases is the most prominent in Gram-negative bacteria (3).  $\beta$ -Lactamases catalyze the hydrolysis of the  $\beta$ -lactam ring to inactivate the drugs. These enzymes are divided into classes A, B, C, and D based on sequence homology. Classes A, C, and D are serine  $\beta$ -lactamases (SBLs) that use a conserved active-site serine to perform nucleophilic attack on the  $\beta$ -lactam ring while class B enzymes are metallo- $\beta$ -lactamases that require one or two zinc ions for catalysis (3).

Class A  $\beta$ -lactamases comprise a large number of enzymes and include penicillinases (*e.g.*, TEM-1 and SHV-1), extended-spectrum  $\beta$ -lactamases (*e.g.*, CTX-M enzymes), and carbapenemases (*e.g.*, SFC-1 and KPC enzymes) (4). Although class A  $\beta$ -lactamases have varying substrate specificity and amino acid sequences ( $\sim$ 30% sequence identity), they use a set of conserved amino acids in the active site for the binding and catalysis of substrates (4). Among these residues, Ser70, which is activated by Lys73, Glu166 and a catalytic water, serves as the nucleophile for attack on the carbonyl carbon of the amide bond of  $\beta$ -lactam substrate (5–7). This results in the breakage of the amide bond and formation of a covalent acyl-enzyme reaction intermediate. During the acylation reaction, a negative charge that develops on the carbonyl oxygen of the reaction intermediate is stabilized by hydrogen bonding interactions with the main chain NH groups of Ser70 and Ser237 and the leaving group nitrogen is protonated by Lys73 *via* a proton shuttle to Ser130 (5). The covalent intermediate is resolved in the deacylation reaction where a catalytic water is activated by the general base Glu166 and attacks the carbonyl carbon of the acyl-enzyme intermediate, thereby releasing the hydrolyzed product (5, 8). In addition, other active-site residues such as Asn132, Asn170, Lys/Arg234, Ser/Thr235 also play important roles in facilitating  $\beta$ -lactam hydrolysis by positioning the catalytic residues or stabilizing the reaction intermediate through hydrogen bonding interactions (4).

\* For correspondence: Timothy Palzkill, [timothy@bcm.edu](mailto:timothy@bcm.edu).

## Structure and mechanism of KPC-44 carbapenemase variant

Many of these catalytically important residues are located on loop structures in the active site such as the 130-loop, omega-loop, 240-loop, and 270-loop (4). However, there is significant variation in the conformations of some active-site loops including the 240-loop and 270-loop that border the active site (Fig. 1).

*Klebsiella pneumoniae* carbapenemase 2 (KPC-2) is a class A  $\beta$ -lactamase with a broad substrate spectrum that includes virtually all  $\beta$ -lactam antibiotics (9). Although first identified in *K. pneumoniae*, the KPC-2 enzyme has been found in multiple bacterial pathogens including *Escherichia coli* (10), *Pseudomonas aeruginosa* (11), and *Acinetobacter* spp. (12). In addition, a number of natural variants of KPC-2 enzyme with amino acid substitutions at residues on the 240-loop and 270-loop have been identified that show altered substrate specificity (13). The global spread of the KPC enzyme is of particular concern as there are limited treatment options for patients infected with KPC-producing bacterial pathogens.

In order to counteract  $\beta$ -lactamase-mediated antibiotic resistance,  $\beta$ -lactamase inhibitors such as clavulanic acid, sulbactam, and tazobactam have been introduced into clinical practice (14) (Fig. 2A). These compounds are  $\beta$ -lactam-based, covalent inactivators that form a stable acyl-enzyme intermediate with the catalytic serine (Ser70) of mainly class A

enzymes. However, these inhibitors can be hydrolyzed by KPC-2 carbapenemase, reducing effectiveness *versus* this enzyme (15).

Avibactam (AVI) is a non- $\beta$ -lactam, diazabicyclooctane inhibitor of SBLs. It forms a covalent, but reversible, carbamoyl bond with the catalytic serine (Ser70) (16, 17) (Fig. 2B). AVI exhibits potent inhibition against a wide range of SBLs including class A, class C, and some class D enzymes and restores the antibacterial activity of  $\beta$ -lactam antibiotics against bacteria expressing these enzymes (18–20). High-resolution crystal structures of AVI in complex with several class A SBLs including SHV-1, KPC-2, and CTX-M enzymes have been determined (21–23). Comparison of these structures reveals that AVI binds in a similar conformation in the active site of the enzymes and forms interactions with multiple key active-site residues including Ser130, Asn132, Lys234, Thr235, and Ser/Thr237, besides forming the carbamoyl linkage with the catalytic Ser70 (Fig. 2B). This indicates that avibactam inhibits these enzymes with a similar carbamylation mechanism (17). In addition, alignment of apo- and AVI-carbamylated structures of CTX-M-14, SHV-1, and KPC-2 revealed that avibactam carbamylation does not cause significant changes in the conformation of active-site residues, indicating that the active site of these enzymes is poised for carbamylation by AVI (21–23).

AVI has been approved in combination with ceftazidime/AVI (CAZ-AVI) as combination therapy for the treatment of complicated urinary tract infections and complicated intra-abdominal infections in the USA (24, 25) and Europe (26). However, there have been reports of resistant bacterial strains in both clinical and laboratory settings since the introduction of CAZ-AVI (27–37). Most of these cases are related to a D179Y substitution in the KPC-2 or KPC-3 enzyme, which yields the KPC-33 and KPC-31 variants, respectively (27, 29, 31, 32, 35, 36). In addition, some resistant variants contain a two amino acid deletion in KPC-2 and KPC-3, which results in KPC-14 and KPC-28, respectively (27, 37) (Fig. S1). However, these mutations also restore susceptibility to carbapenems as they abolish the carbapenemase activity of KPC-2 and KPC-3 variants (29, 32, 35–37).

KPC-44 is a recently identified KPC variant with a duplication of 15 amino acids (Ala262 to Glu276) on the 270-loop of KPC-2 (30) (Fig. S1). It occurred after prolonged CAZ-AVI treatment of a patient colonized with KPC-2-producing *K. pneumoniae* (30). Antimicrobial susceptibility tests indicated that KPC-44 was associated with CAZ-AVI resistance in the *K. pneumoniae* isolate. In addition, the KPC-44-producing *K. pneumoniae* strain was also resistant to carbapenems (e.g., meropenem), although at a lower level than that of the parental KPC-2-producing strain. We sought to determine the molecular basis of KPC-44-mediated resistance by examining  $\beta$ -lactam hydrolysis and AVI carbamylation by the KPC-44 enzyme. We found that the KPC-44 variant retains penicillinase and carbapenemase activity and exhibits CAZ-AVI resistance by increasing the rate of CAZ hydrolysis and decreasing AVI carbamylation efficiency. We also determined the X-ray crystal structures of the KPC-44 apo enzyme and the

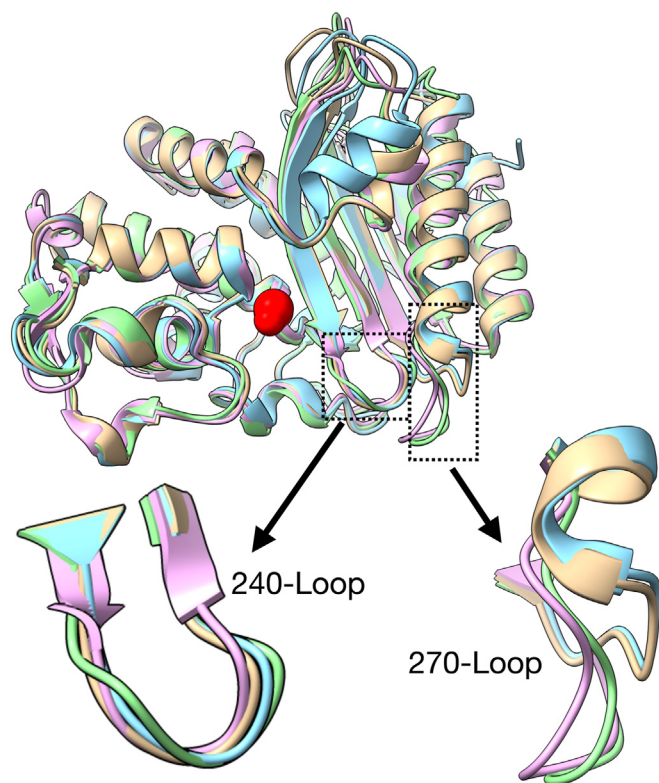


**Figure 1.** Comparison of X-ray crystal structures of TEM-1 (PDB ID: 1ZG4, tan), SHV-1 (PDB ID: 4FH4, green), CTX-M-14 (PDB ID: 1YLT, orchid), and KPC-2  $\beta$ -lactamases (PDB ID: 5UL8, cyan). The 240-loop and 270-loop are boxed and enlarged versions are shown indicated by arrows. The catalytic residue Ser70 is shown in red sphere. KPC, *Klebsiella pneumoniae* carbapenemase; PDB, Protein Data Bank.

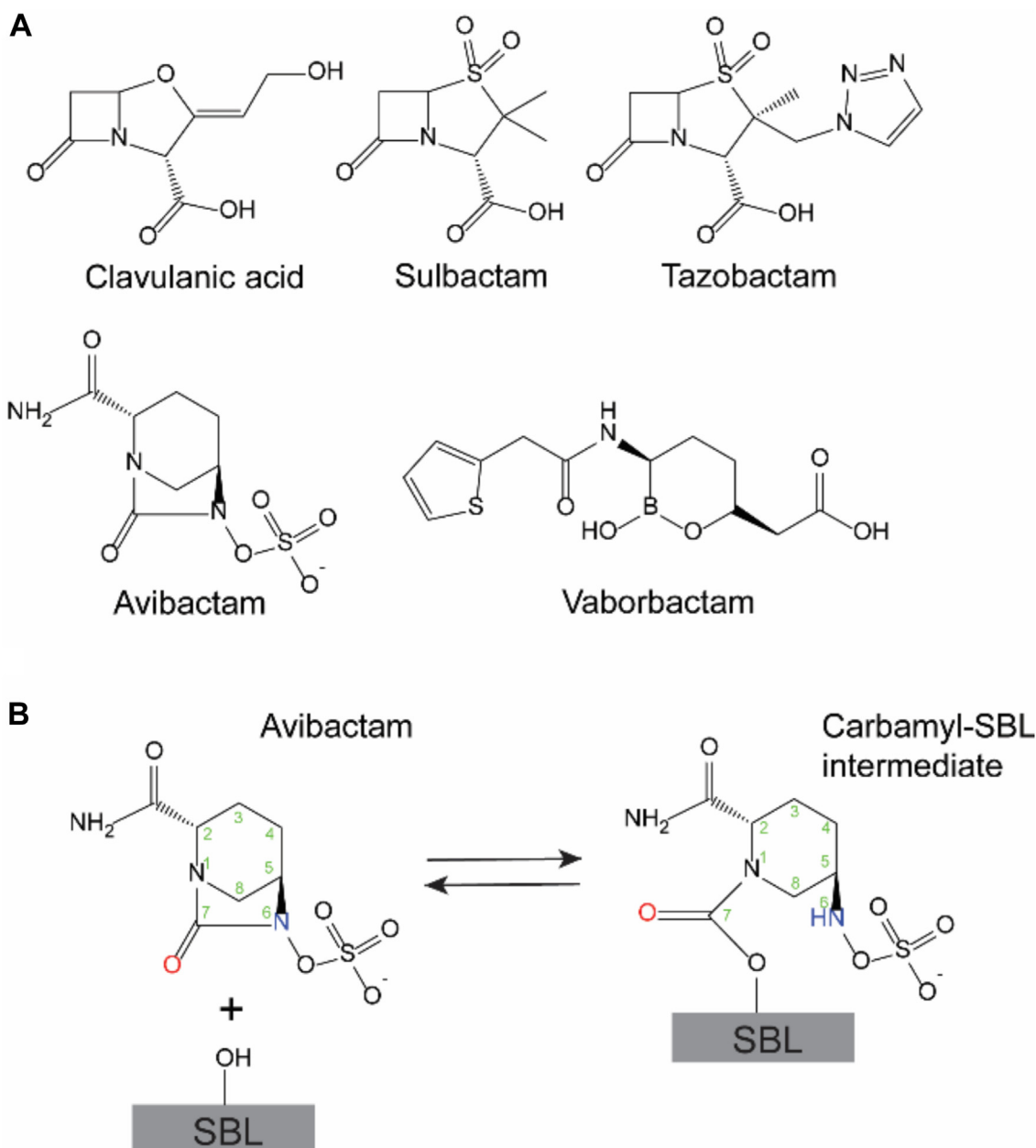


**Figure 2. Chemical structures of  $\beta$ -lactamase inhibitors.** A,  $\beta$ -lactamase inhibitor structures and (B) the scheme for avibactam inhibition of serine  $\beta$ -lactamases.

covalent complex of KPC-44 with AVI, which indicates that CAZ-AVI resistance associated with the KPC-44 variant may occur through modulating the stability and conformations of the 240-, 270-, and omega-loops.

## Results

### KPC-44 confers reduced CAZ and CAZ/AVI susceptibility than KPC-2

To investigate whether *bla*<sub>KPC-44</sub> accounts for the CAZ/AVI resistance phenotype observed in the *K. pneumoniae* clinical isolate (30), both *bla*<sub>KPC-2</sub> and *bla*<sub>KPC-44</sub> were individually expressed in *E. coli* and their CAZ/AVI minimum inhibitory concentrations (MICs) were compared. The levels of CAZ

resistance provided by the KPC-2 and KPC-44 enzymes were determined by measuring MICs of CAZ for KPC-2- or KPC-44-expressing bacterial cells in the absence and presence of 4  $\mu$ g/ml AVI, which is the concentration used in the combination therapy.

As shown in Table 1, expression of the KPC-2 enzyme in *E. coli* cells resulted in a 4-fold increase in CAZ MIC *versus* that provided by the vector alone control. However, this increase was abolished when AVI was used together with CAZ, indicating that the KPC-2 enzyme was inhibited by AVI. Expression of the KPC-44 enzyme conferred a 16-fold higher CAZ MIC than the negative control and 4-fold higher than observed with WT KPC-2 (Table 1). The addition of AVI lowered the CAZ MIC by 4-fold. However, this level is

## Structure and mechanism of KPC-44 carbapenemase variant

**Table 1**

Minimum inhibitory concentrations of  $\beta$ -lactams against *Escherichia coli* expressing KPC-2 or KPC-44

$\beta$ -lactam antibiotics	MIC ( $\mu$ g/ml)		
	Vector control	KPC-2	KPC-44
Ceftazidime	0.5	2	8
Ceftazidime/avibactam	0.5	0.5	2
Ampicillin	4	128	64
Imipenem	0.25	1.5	0.75
Meropenem	0.25	0.375	0.25

KPC, *Klebsiella pneumoniae* carbapenemase.

equivalent to that observed for WT KPC-2 in the absence of AVI. Therefore, the expression of KPC-44 increases the MIC levels for *E. coli* for CAZ/AVI relative to that observed for *E. coli* with KPC-2, similar to observations with *K. pneumoniae* clinical isolates (30).

### KPC-44 variant retains both ampicillin and imipenem susceptibility similar to KPC-2

CAZ-AVI-resistant KPC variants containing the D179Y mutation, such as KPC-31 and KPC-33, lack penicillin and carbapenem resistance (29, 32, 36, 38). In contrast, the *K. pneumoniae* clinical isolate containing KPC-44 is reported to retain penicillin and carbapenem resistance, although it is lower than that provided by the WT KPC-2 enzyme (30). Therefore, we examined both penicillin and carbapenem resistance levels of *E. coli* expressing KPC-44.

As shown in Table 1, KPC-44 conferred reduced ampicillin susceptibility to *E. coli* cells, although it is 2-fold lower than that provided by WT KPC-2. In addition, *E. coli* expressing KPC-44 exhibited 3-fold increased imipenem MICs when compared with the no  $\beta$ -lactamase control strain. However, the KPC-44-mediated imipenem MIC was 2-fold lower than the MIC for KPC-2-expressing cells (Table 1). Neither KPC-2 nor KPC-44 conferred significant meropenem MIC levels to *E. coli* cells. Therefore, KPC-44 provides at least partially reduce ampicillin and imipenem susceptibility compared to strains expressing KPC-2. Note that the MIC values for meropenem in our experiments are well below those reported for

the *K. pneumoniae* clinical isolates containing KPC-2 or KPC-2, which were >32 and 16  $\mu$ g/ml, respectively (30). The difference is likely due to the use of a laboratory strain of *E. coli* and a recombinant plasmid with a different promotor for KPC expression than that occurring with natural isolates.

### KPC-44 enzyme displays faster CAZ hydrolysis but slower carbapenem hydrolysis than WT KPC-2

$\beta$ -lactamase-mediated  $\beta$ -lactam resistance is strongly influenced by the rate of drug hydrolysis. Therefore, kinetic parameters for KPC-2 and KPC-44 hydrolysis were determined for a representative penicillin, ampicillin, the carbapenems, imipenem, and meropenem, as well as CAZ (Table 2) (30).

Steady-state kinetic analysis of CAZ hydrolysis by the KPC-2 and KPC-44 enzymes showed  $K_M$  was too high to be accurately determined (Table 2). However, fitting of the progress curve for CAZ hydrolysis revealed that KPC-44 has a 5-fold higher  $k_{cat}/K_M$  value than that for the KPC-2 enzyme (Table 2). Kinetic parameters for ampicillin hydrolysis by KPC-44 were comparable to those observed with the KPC-2 enzyme (Table 2). In contrast,  $k_{cat}$  and  $k_{cat}/K_M$  for KPC-44 hydrolysis of imipenem were 8-fold and 4-fold lower than those of the KPC-2 enzyme, respectively (Table 2). Similarly,  $k_{cat}$  and  $k_{cat}/K_M$  values for meropenem hydrolysis by KPC-44 were 7-fold and 3-fold lower than those of the KPC-2 enzyme, respectively (Table 2). This indicates that KPC-44 hydrolyzes carbapenems, albeit at a slower rate than KPC-2. These kinetics results are consistent with the MIC results for *E. coli* expressing the KPC-2 and KPC-44 enzymes (Table 1).

### KPC-44 exhibits lower AVI carbamylation efficiency than KPC-2 enzyme

Susceptibility testing of *E. coli* and *K. pneumoniae* expressing KPC-2 or KPC-44 showed that AVI increases CAZ susceptibility levels to background of the no  $\beta$ -lactamase control for the KPC-2 enzyme but not the KPC-44 variant (27, 30, 37). Therefore, we examined AVI inhibition of the KPC-2 and KPC-44 enzymes. Because CAZ is a poor substrate for KPC-2 and KPC-44, we used the colorimetric substrate

**Table 2**

Kinetic parameters for  $\beta$ -lactam antibiotic hydrolysis by KPC-2 and KPC-44

Substrate	Kinetic parameters	Enzyme	
		KPC-2	KPC-44
Ceftazidime	$k_{cat}$ ( $s^{-1}$ )	>0.8	>1.5
	$K_M$ ( $\mu$ M)	>600	>600
	$k_{cat}/K_M$ ( $\mu M^{-1} s^{-1}$ )	0.0011 $\pm$ 0.000066	0.0057 $\pm$ 0.00031
Ampicillin	$k_{cat}$ ( $s^{-1}$ )	160 $\pm$ 10	126 $\pm$ 5
	$K_M$ ( $\mu$ M)	210 $\pm$ 33	232 $\pm$ 22
	$k_{cat}/K_M$ ( $\mu M^{-1} s^{-1}$ )	0.76 $\pm$ 0.13	0.54 $\pm$ 0.056
Imipenem	$k_{cat}$ ( $s^{-1}$ )	50 $\pm$ 4.5	6.4 $\pm$ 0.33
	$K_M$ ( $\mu$ M)	130 $\pm$ 33	57 $\pm$ 7.1
	$k_{cat}/K_M$ ( $\mu M^{-1} s^{-1}$ )	0.38 $\pm$ 0.10	0.11 $\pm$ 0.015
Meropenem	$k_{cat}$ ( $s^{-1}$ )	3.3 $\pm$ 0.18	0.46 $\pm$ 0.022
	$K_M$ ( $\mu$ M)	19 $\pm$ 2.9	7.3 $\pm$ 1.4
	$k_{cat}/K_M$ ( $\mu M^{-1} s^{-1}$ )	0.17 $\pm$ 0.028	0.063 $\pm$ 0.012
Nitrocefin	$k_{cat}$ ( $s^{-1}$ )	130 $\pm$ 2.2	20 $\pm$ 0.67
	$K_M$ ( $\mu$ M)	45 $\pm$ 2.1	16 $\pm$ 1.4
	$k_{cat}/K_M$ ( $\mu M^{-1} s^{-1}$ )	2.9 $\pm$ 0.14	1.3 $\pm$ 0.12

KPC, *Klebsiella pneumoniae* carbapenemase.



nitrocefin to assess AVI inhibition potency for the enzymes. Accordingly, varying concentrations of AVI were preincubated with the KPC enzymes before adding nitrocefin to start the reaction. We found that AVI inhibited nitrocefin hydrolysis by KPC-2 with an  $IC_{50}$  of  $0.027 \pm 0.0015 \mu\text{M}$  (Table 3). In contrast, the  $IC_{50}$  of AVI for KPC-44 was  $0.21 \pm 0.007 \mu\text{M}$  (Table 3). Therefore, inhibition by AVI is approximately 8-fold less potent *versus* KPC-44 compared to the KPC-2 enzyme.

AVI inhibits SBLs, including KPC-2, by forming a carbamoyl linkage with the catalytic serine (Ser70) of  $\beta$ -lactamases (16, 17, 23) (Fig. 2B). Based on the mechanism, the carbamylation efficiency ( $k_2/K_i$ ) of AVI is a critical determinant of the AVI sensitivity of  $\beta$ -lactamases. Therefore,  $k_2/K_i$  of AVI for KPC-2 and KPC-44 enzymes was evaluated based on the inhibition of nitrocefin hydrolysis by AVI for a two-step reaction, as described previously (16, 17). Fitting of the progress curves of nitrocefin hydrolysis yielded  $k_{obs}$  values at varying concentrations of AVI. After fitting of the  $k_{obs}$  values to Equation 2 (Experimental procedures), the  $k_2/K_i$  values of AVI for KPC-2 and KPC-44 were determined as  $6800 \pm 160$  and  $550 \pm 4.6 \text{ M}^{-1} \text{ s}^{-1}$ , respectively (Table 3). Therefore, the KPC-44 variant exhibits a 12-fold reduction in the AVI carbamylation efficiency compared to KPC-2, which may account for its observed reduction in AVI susceptibility and increased  $IC_{50}$  for AVI.

AVI carbamylation of SBLs has been observed to be reversible, which results in the recyclization of the diazabicyclooctane ring of AVI and the liberation of free enzyme (16, 17) (Fig. 2B). Therefore, the rates of AVI decarbamylation ( $k_{-2}$ ) from carbamylated KPC-2 and KPC-44 enzymes were also determined by jump dilution where avibactam and KPC enzyme were incubated for 2 h and subsequently diluted 100-fold into buffer with nitrocefin. Nitrocefin hydrolysis was monitored to evaluate the rate of recovery of the free enzyme from the AVI-inhibited form. By fitting the progress curve of nitrocefin hydrolysis to Equation 2 (Experimental procedures), the  $k_{-2}$  of carbamylated AVI was determined as  $(9.6 \pm 0.020) \times 10^{-5}$  and  $(7.1 \pm 0.32) \times 10^{-5} \text{ s}^{-1}$  for KPC-2 and KPC-44, respectively (Table 3). Therefore, the rate of AVI decarbamylation for KPC-44 is similar to that of KPC-2 enzyme.

#### KPC-44 is more sensitive to inhibition by clavulanate but equally sensitive to vaborbactam compared to KPC-2

We next determined the  $IC_{50}$  for clavulanate inhibition of KPC-44 and found it was 7-fold more sensitive to inhibition by

clavulanate than the KPC-2 enzyme, with an  $IC_{50}$  value of  $4.8 \mu\text{M}$  *versus*  $32 \mu\text{M}$  (Table 3). Therefore, the 15 amino acid insertion on the 270-loop of KPC-44 sensitizes the enzyme to clavulanate inhibition.

Vaborbactam is another potent, reversible covalent inhibitor for a broad range of SBLs including the KPC-2 enzyme (39). It is a cyclic boronic acid (Fig. 2) and functions by forming a reversible borylation linkage with Ser70 of target enzymes (39). It has been reported that the potency of vaborbactam is much less affected than that for AVI by the D179Y substitution (40). Similarly, we observed a less than 2-fold difference in the vaborbactam  $IC_{50}$  value for KPC-44 compared to KPC-2 (Table 3). Furthermore, we determined the vaborbactam borylation efficiency ( $k_2/K_i$ ) and deborylation rate ( $k_{-2}$ ) for the KPC-2 and KPC-44 enzymes, which showed a 4-fold lower  $k_2/K_i$  and a 3-fold higher  $k_{-2}$  for KPC-44 than KPC-2, which is broadly consistent with the moderately higher  $IC_{50}$  value for KPC-44.

#### Fifteen amino acid repeat alters conformations of the 240- and 270-loops of the KPC-44 enzyme

To understand the molecular basis for the differences in  $\beta$ -lactam hydrolysis rates and AVI potency for the KPC-2 and KPC-44 enzymes, the structure of the KPC-44 apo-enzyme was determined by X-ray crystallography to 1.26 Å resolution. We determined the structure in the presence and absence of the cryoprotectant, ethylene glycol. It is noteworthy that six amino acids (Lys270–Ser275) in the region of the 15 amino acid repeat (Ala262–Glu291) lack electron density, suggesting the region is flexible (Figs. 2 and 3). A further indication of flexibility in this region is the very high B-factors for the 270-loop region (Fig. S2). In addition, in the absence of cryoprotectant, the structure of this region is more disordered and 14 residues (Lys270–Pro283) lack electron density (Fig. S3).

A structural alignment of KPC-44 and KPC-2 apo-enzymes (RMSD = 0.395 Å) revealed that most of the key catalytic residues, including Lys73, Ser130, and Glu166, adopt the same conformation in both the enzymes (Fig. 4, A–C). In addition, the catalytic water is coordinated in a similar position in the active sites of KPC-2 and KPC-44 by forming hydrogen bonds with Ser70, Glu166, and Asn170 (Fig. 4, A–C). Also, as noted, Lys270–Glu275 are unstructured, and thus KPC-44 lacks a defined structure of the 270-loop region (Fig. 3C). Besides the 270-loop region with the 15 amino acid repeat, there are also changes in the conformation of the Cys238 to Gly242 loop

**Table 3**  
KPC-2 and KPC-44  $\beta$ -lactamase inhibition parameters

Inhibitor	Inhibition constant	Enzyme	
		KPC-2	KPC-44
Avibactam	$IC_{50}$ ( $\mu\text{M}$ )	$0.027 \pm 0.0015$	$0.21 \pm 0.0070$
	$k_2/K_i$ ( $\text{M}^{-1} \text{s}^{-1}$ )	$6800 \pm 160$	$550 \pm 4.6$
	$k_{-2}$ ( $\text{s}^{-1}$ )	$(9.6 \pm 0.020) \times 10^{-5}$	$(7.1 \pm 0.32) \times 10^{-5}$
Vaborbactam	$IC_{50}$ ( $\mu\text{M}$ )	$0.13 \pm 0.0054$	$0.22 \pm 0.00092$
	$k_2/K_i$ ( $\text{M}^{-1} \text{s}^{-1}$ )	$1200 \pm 230$	$320 \pm 16$
	$k_{-2}$ ( $\text{s}^{-1}$ )	$(1.2 \pm 0.014) \times 10^{-5}$	$(2.9 \pm 0.047) \times 10^{-5}$
Clavulanate	$IC_{50}$ ( $\mu\text{M}$ )	$32 \pm 3.1$	$4.8 \pm 0.17$

KPC, *Klebsiella pneumoniae* carbapenemase.

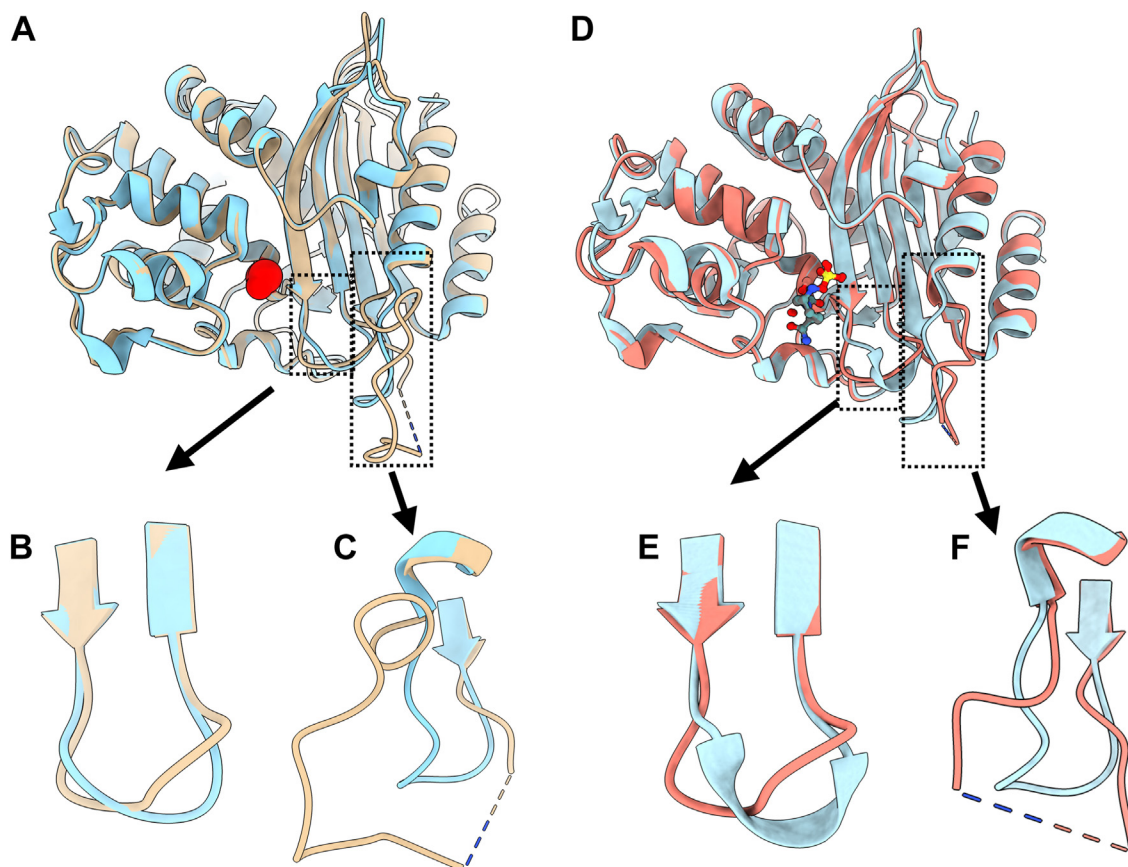


**Figure 3. Schematic illustrations of KPC-2 and KPC-44 structures in apo-form and in complex with avibactam.** A, structural alignment of KPC-2 (blue) (PDB id: 2OV5) and KPC-44 (tan) apo-enzymes. The 240- and 270-loops are boxed. The catalytic residue Ser70 is shown in red sphere. B, 240-loop region of KPC-2 and KPC-44 apo-enzymes. C, 270-loop region of KPC-2 and KPC-44 apo-enzymes. D, structural alignment of KPC-2 in complex with avibactam (blue) (PDB id: 4ZBE) and KPC-44 in complex with avibactam (salmon). E, 240-loop region of KPC-2 and KPC-44 in complex with avibactam. F, 270-loop region of KPC-2 and KPC-44 in complex with avibactam. KPC, *Klebsiella pneumoniae* carbapenemase; PDB, Protein Data Bank.

(240-loop) (Figs. 3, A and B, and 5). The side chains of residues within the loop adopt different conformations, particularly the orientation of the side chain of Tyr241, which is directed toward the active site in KPC-2 but not in KPC-44 (Fig. 5, A and C). The 240-loop conformation is stabilized in KPC-2, in part, by hydrogen bonds between the main chain N of Tyr241 and the main chain O atoms of Lys270 and the main chain O of Asp272 and main chain N of Gly242, which are lost in KPC-44 because of the structural disorder of region Lys270 to Ser275. In addition, there are numerous van der Waals packing contacts between the 240- and 270-loops and the majority of these contacts are lost in KPC-44 due to disorder in the 270-loop (Fig. 5, B and D). Therefore, the duplication of 15 amino acid residues after Glu276 of KPC-2, which creates the KPC-44 variant, not only results in conformational changes in the local region (270-loop) but also the loop region of Thr237 to Gly242 (240-loop) by altering hydrogen bonding and packing interactions.

The disorder in the 270-loop also propagates to decrease stabilizing interactions between the 240-loop and the active-site omega loop that contains the key active-site residues Glu166 and Asn170. There are numerous van der Waals interactions between the 240-loop and the Asn170 to Pro174 residues of the omega loop in the KPC-2 enzyme (Fig. 5B).

Many of these interactions are lost due to the altered conformation of the 240-loop in the KPC-44 enzyme (Fig. 5D). The loss of these contacts may lead to destabilization of the omega loop in KPC-44 relative to KPC-2 and could thereby alter enzyme activity.

The propagation of structural changes from the insertion in the 270-loop to the omega loop could provide a rationale for the observation that KPC-44 exhibits a 5-fold higher  $k_{cat}/K_M$  value than KPC-2 in hydrolyzing CAZ but a 4-fold lower  $k_{cat}/K_M$  value than KPC-2 in hydrolyzing imipenem (Table 2). The structure of a deacylation-deficient mutant of KPC-2 (KPC-2 E166Q) was recently determined in the apo form and in acyl-enzyme covalent complex with CAZ (41). Structural alignment of KPC-44 with KPC-2 E166Q apo and in complex with CAZ revealed conformational variations in the omega-, 240-, and 270-loops among the three structures. Although the omega-loop adopts same conformation in the KPC-2 E166Q apo enzyme and KPC-44, it is disordered in KPC-2 E166Q/CAZ, as are the 240- and 270-loops (Fig. S4) (41). The disordered omega loop avoids the steric clash of Asn170 on the loop with the aminothiazole ring of the C7 substituent of CAZ (41). We speculate that a similar disordering of the omega loop occurs during CAZ hydrolysis by KPC-44 (41). The transition to the disordered loop is likely facilitated by the loss of stabilizing

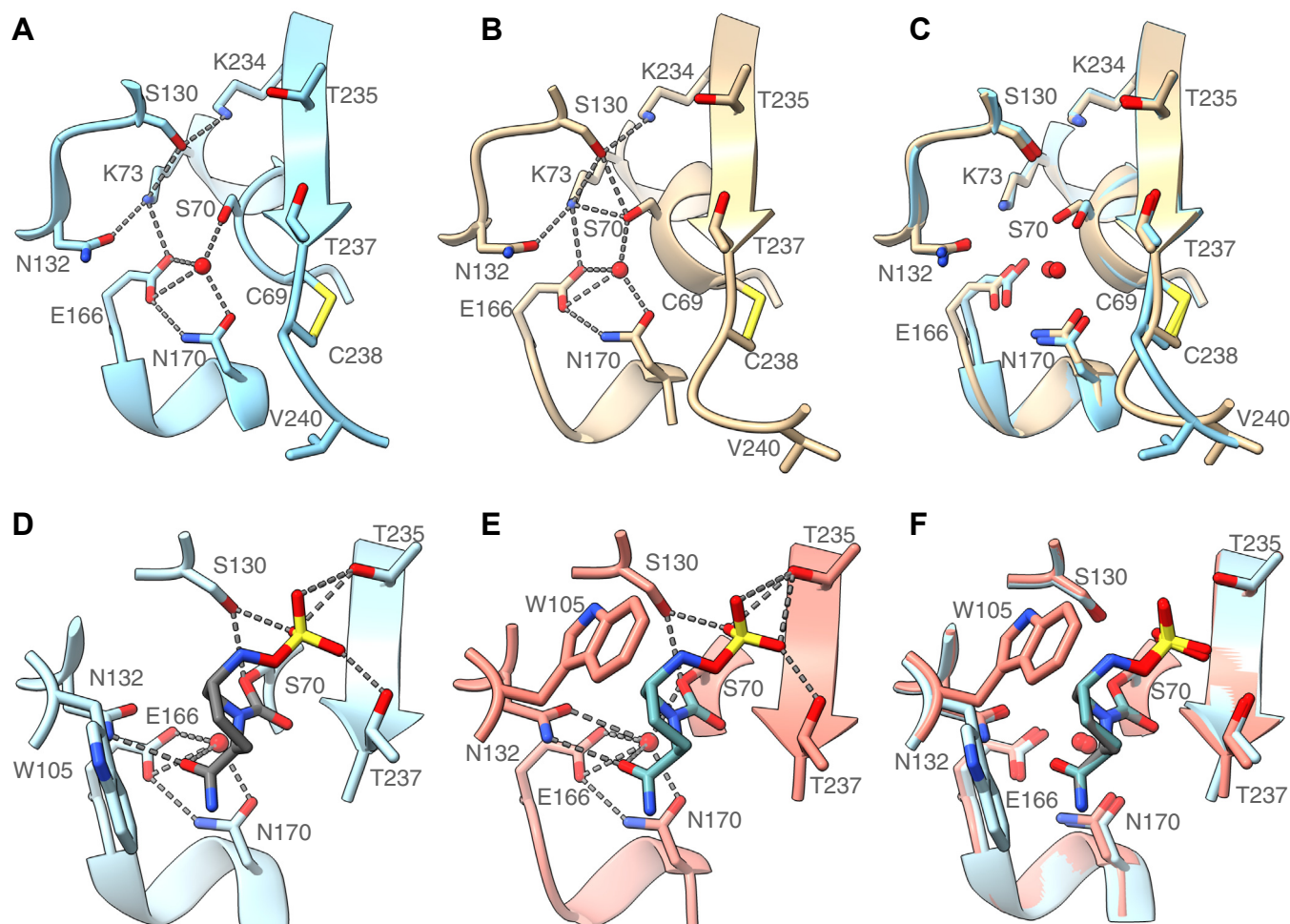


**Figure 4. Schematic illustration of active site region of KPC-2 and KPC-44  $\beta$ -lactamases in apo- and avibactam bound forms.** A, active site of KPC-2  $\beta$ -lactamase apo-enzyme (blue) (PDB id: 2OV5). Residue positions are labeled and hydrogen bonds are shown as dashed lines. Water is shown as a red sphere. Oxygen is shown in red, nitrogen in blue, and sulfur in yellow. B, active site of KPC-44  $\beta$ -lactamase apo-enzyme (tan). C, structural alignment of the active sites of KPC-2 and KPC-44. Hydrogen bonds are omitted for clarity. D, active site of KPC-2  $\beta$ -lactamase (light blue) in complex with avibactam (gray) (PDB id: 4ZBE). E, active site of KPC-44  $\beta$ -lactamase (salmon) in complex with avibactam (green). F, structural alignment of the active sites of KPC-2 and KPC-44 in complex with avibactam. Hydrogen bonds are omitted for clarity. KPC, *Klebsiella pneumoniae* carbapenemase; PDB, Protein Data Bank.

contacts between the 240-loop and the omega loop in KPC-44 (Fig. 5). A similar mechanism has been proposed for the action of the D179Y substitution in the CAZ/AVI variants containing this substitution (42). The movement of the Glu166 general base away from a position to activate the deacylation water in the disordered loop was suggested to be compensated for by substrate-assisted catalysis by the ring nitrogen of the aminothiazole ring of CAZ, which would be in a position to activate the water (42). By a similar reasoning, destabilizing the omega loop could alter the positioning of the Glu166 general base, leading to reduced hydrolysis activity for imipenem, which does not have a group positioned for substrate-assisted catalysis.

To further investigate if the insertion in the 270-loop affects active site flexibility and dynamics, we performed molecular dynamics (MD) simulations on the KPC-2 and KPC-44 apo-enzymes. The simulations were done for 100 ns with three replicate simulations for each enzyme. Considering all replicate simulations, the overall average RMSD for KPC-2 was 1.88 Å (SD = 0.02) while that for KPC-44 was 3.54 Å (SD =

0.06) (Fig. S6A). This indicates more variation in the positions of atoms in KPC-44 versus KPC-2 during the simulations, consistent with a more flexible enzyme. We also examined the distance variations between key active-site residues during the simulations (Table S2 and Fig. S7). It is noteworthy that the distance between the Ser70(OG) and Glu166(CD) and between Ser70(OG) and Asn170(CG) is consistently shorter for KPC-44 than KPC-2, suggesting the insertion in the 270-loop alters the position of the omega loop. Also, for all of the average distances between active-site atoms shown in Table S2, the SD of the distances is higher for KPC-44 than KPC-2. Thus, for the distances examined, KPC-44 samples a wider range of distances than KPC-2 during the simulations, particularly for distances involving the omega loop. Finally, we examined the rms fluctuation values for the residues of the KPC-2 and KPC-44 enzymes from the simulations (Fig. S6B). The results show the 270-loop region of KPC-44 has much higher values than observed with KPC-2, consistent with the inserted residues being flexible (Fig. S6B). Further, examination of the Arg164-Asp179 omega-loop residues reveals higher values for KPC-



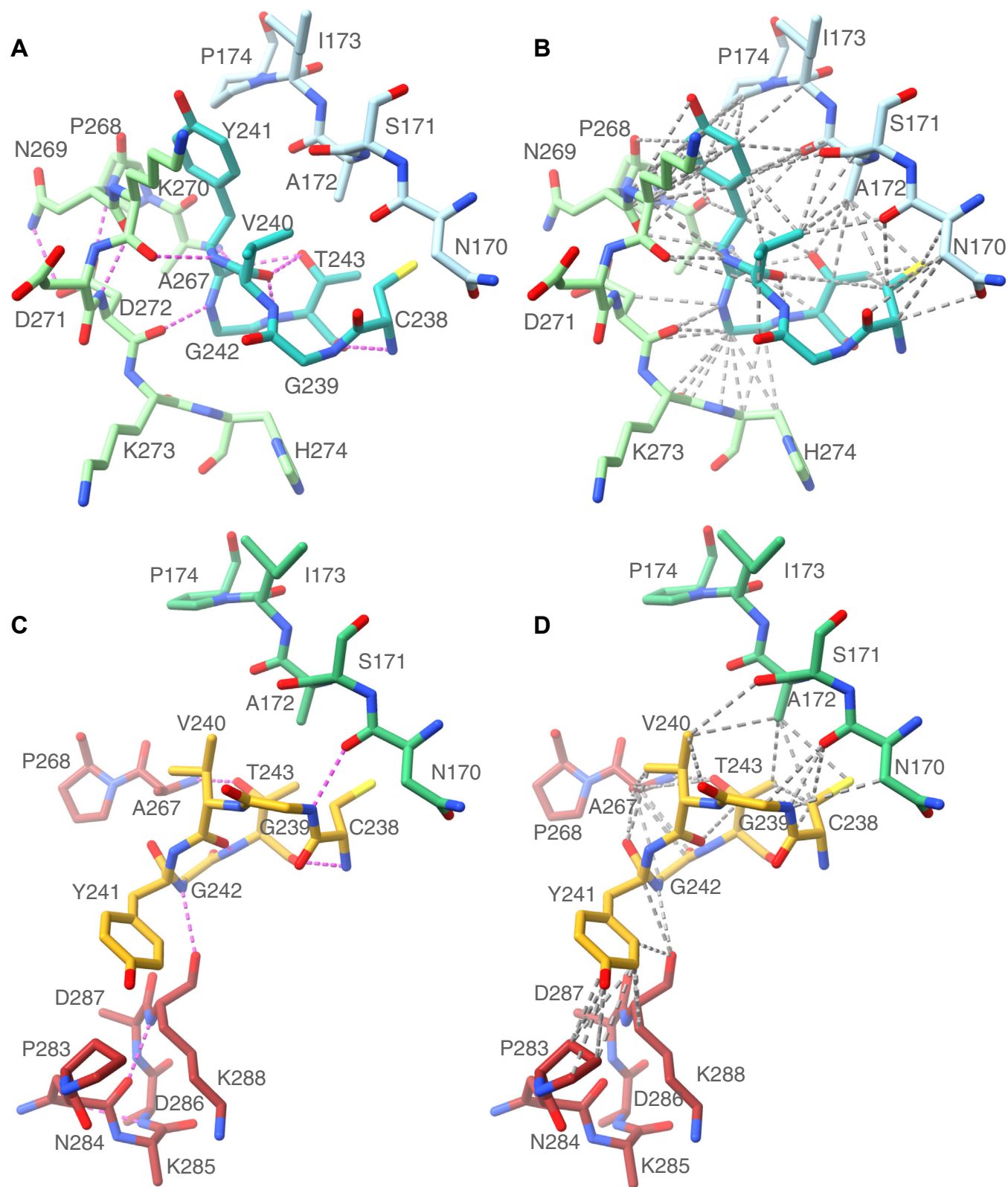


**Figure 5. Hydrogen bond and van der Waals interactions between the omega, 240-, and 270-loops in KPC-2 and KPC-44.** A, hydrogen bond interactions between the omega, 240-, and 270-loop regions in KPC-2  $\beta$ -lactamase. Relevant omega loop residues are colored *light blue*, 240-loop residues are *blue-green*, and 270-loop residues are *light green*. Nitrogen is shown in *blue* and oxygen in *red*. The residue positions are indicated in *black*. Hydrogen bonds are shown with *pink dashed lines*. B, van der Waals interactions between omega, 240-, and 270-loop regions in KPC-2. Contacts at 4 Å are shown in *gray dashed lines*. C, hydrogen bond interactions between the omega, 240-, and 270-loop regions in KPC-44  $\beta$ -lactamase. Relevant omega loop residues are colored *green*, 240-loop residues are in *gold*, and 270-loop residues are *brown*. Hydrogen bonds are shown as *pink dashed lines*. Note the altered conformations of the 240- and 270-loops in KPC-44 versus KPC-2. D, van der Waals interactions between omega, 240-, and 270-loop regions in KPC-44. Contacts at 4 Å are shown in *gray dashed lines*. KPC, *Klebsiella pneumoniae* carbapenemase.



44 than KPC-2, consistent with enhanced flexibility of the omega loop in KPC-44 (Fig. S6C). Taken together, the MD results are consistent with the hypothesis that the 270-loop and omega loop are more mobile in KPC-44 than KPC-2, which could facilitate the binding of CAZ.

**Both AVI carbamylation and vaborbactam borylation in the active site of KPC-44 variant cause further disorder in the 270-loop of the protein**

Kinetic analysis of the inhibition of KPC-2 and KPC-44 enzymes by AVI and vaborbactam demonstrated that the AVI acylation efficiency and vaborbactam borylation efficiency of KPC-44 variant are 12-fold and 4-fold lower than that of KPC-2 enzyme, respectively (Table 3). To understand the molecular mechanism underlying these differences, the protein crystals of the KPC-44 variant were soaked with saturating concentrations of AVI (10 mM) or vaborbactam (5 mM) to determine the structure of the KPC-44 variant in complex with these inhibitors.

The structure of the KPC-44/AVI complex was determined to 1.37 Å resolution. The presence of AVI did not change the space group ( $P32_1$ ) of the crystals. One molecule of AVI was found to form a covalent bond with the side chain hydroxyl group of Ser70 and was refined as an occupancy of 1 (Figs. 4E, 6, and S5). The polder map shows difference density for the covalently linked AVI (Fig. S8A). The C2 carboxamide group forms a hydrogen bond with the side chain amine group of Asn132 (Fig. 4E). The N6 sulfate group hydrogen bonds with the side chains of Ser130, Thr235, and Thr237, while the piperidine ring forms a  $\pi$ - $\pi$  interaction with the side chain of Trp105 (Fig. 4E). In addition, the C7 carbonyl oxygen is present in the oxyanion hole and forms hydrogen bonds with main chain N of Ser70 and Thr237.

Structural alignment of KPC-44/AVI with the KPC-44 apo-enzyme reveals that AVI carbamylation alters the conformation of the side chain of Trp105 (Fig. 4E), which can be

attributed to its interaction with the piperidine ring of AVI. More notably, the region with the 15 amino acid residues repeat (Ala262-Glu291) is more disordered in the KPC-44/AVI structure than in the apo structure in that 15 residues (Lys270-Asn284) cannot be modeled, suggesting that carbamylation of KPC-44 with AVI further increases the flexibility of the 270-loop. Of note, residues Asp276 to Asn284 in the structures of KPC-44 crystals with short soaking times (<2 h) and no AVI complex, could be modeled in the same conformation as that found in the structure of KPC-44 crystals not exposed to AVI. This suggests that disorder of residues Asp276 to Asn284 in the structure of KPC-44/AVI complex is caused by the binding and/or carbamylation of AVI in the active site. Finally, the structure of AVI in complex with KPC-44 is superimposable with the KPC-2/AVI structure (Figs. 4, D and E and 6). This finding is consistent with the fact that the decarbamylation rate ( $k_{-2}$ ) is the same for KPC-2 and KPC-44 (Table 3).

The structure of KPC-44 enzyme in complex with vaborbactam was determined to 1.70 Å resolution (Table S1). One molecule of vaborbactam, refined to occupancy of 1.0, was observed in the active site of KPC-44 in covalent linkage with Ser70 *via* the boron atom and a polder map shows density for the bound vaborbactam (Figs. 7 and S8B). The carboxylate group of vaborbactam forms hydrogen bonds with side chain hydroxyl groups of Ser130, Thr235, and Thr237 (Fig. 7B). The exocyclic hydroxyl oxygen of the cyclic boronic acid is located in the oxyanion hole and forms hydrogen bonds with main chain amide groups of both Ser70 and Thr237 while the endocyclic oxygen forms a hydrogen bond with the main chain amide of Ser237 (Fig. 7B). The exocyclic oxygen also forms hydrogen bonds with the deacylation water and the side chain oxygen of Asn170. Further, the amide group and carbonyl oxygen of vaborbactam form hydrogen bonds with the main chain oxygen of Thr237 and side chain nitrogen of Asn132, respectively (Fig. 7B). In addition, the cyclic boronic acid ring of vaborbactam makes hydrophobic interactions with the side chain of Trp105 of KPC-44 as does the five-membered

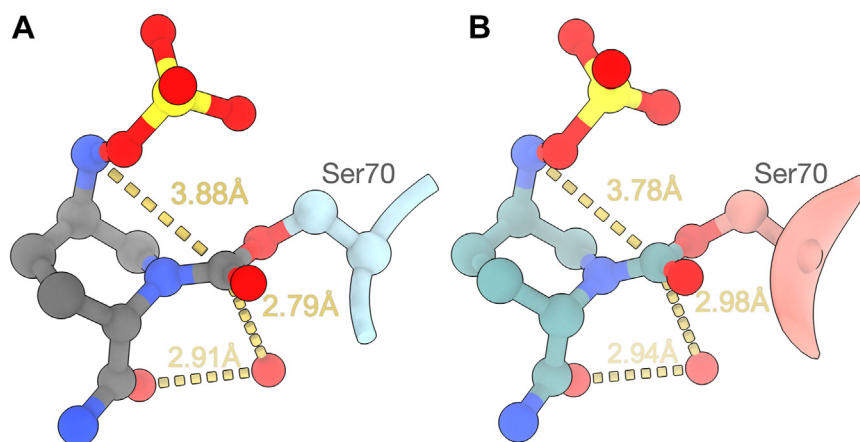


**Figure 6. Schematic illustration of acyl-enzyme structures of KPC-2 and KPC-44 with avibactam.** A, structure of KPC-2  $\beta$ -lactamase (blue) acyl-enzyme complex with avibactam (gray) (PDB id: 4ZBE). The catalytic water is shown as a red sphere. Oxygen is in red, nitrogen in blue, and sulfur in yellow. Distances are shown in yellow dashes and are labeled. B, structure of KPC-44  $\beta$ -lactamase (salmon) acyl-enzyme complex with avibactam (green). KPC, *Klebsiella pneumoniae* carbapenemase; PDB, Protein Data Bank.

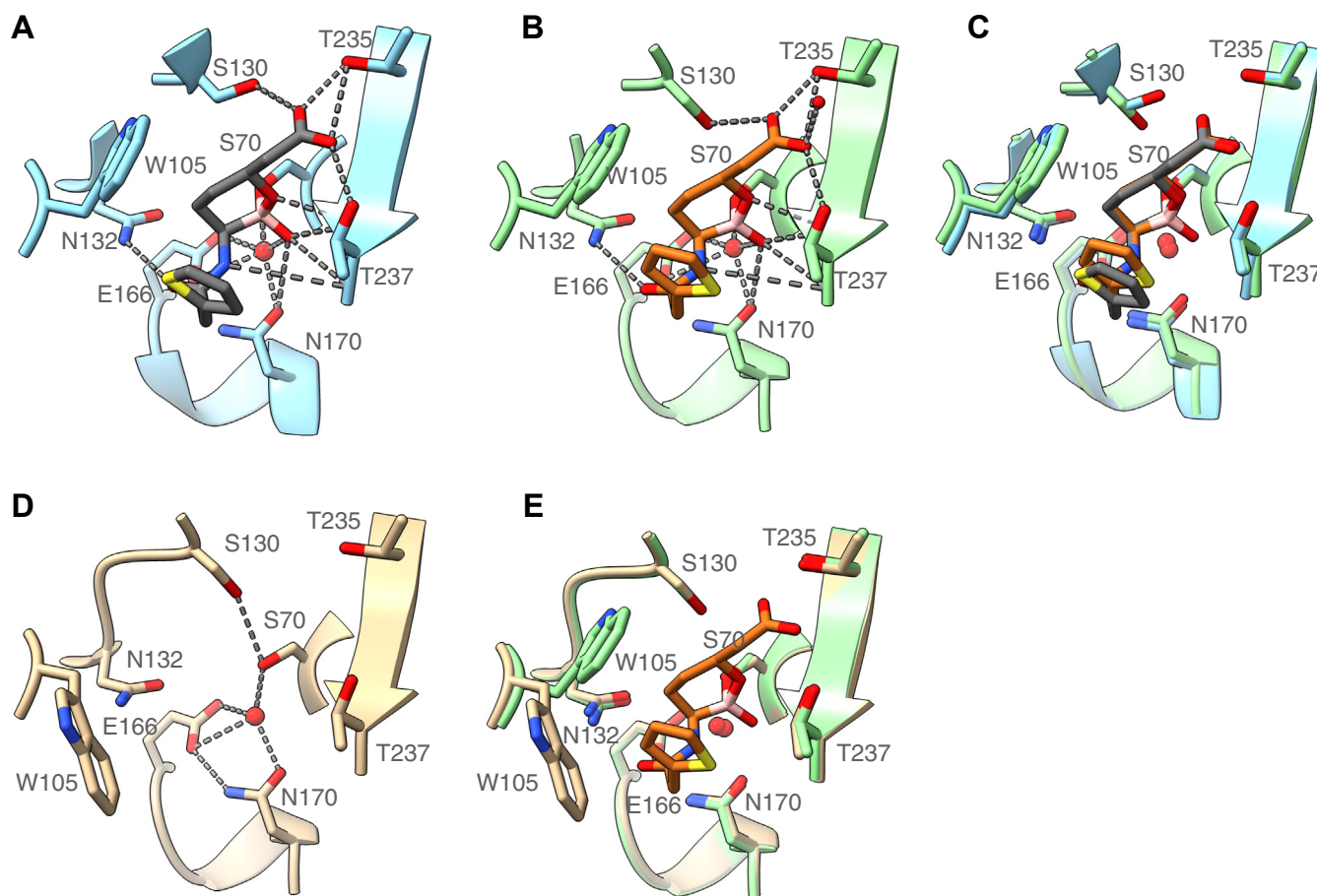


**Figure 7. Schematic illustration of KPC-2 and KPC-44  $\beta$ -lactamases in complex with vaborbactam.** A, structure of KPC-2  $\beta$ -lactamase (light blue) in complex with vaborbactam (gray) (PDB id: 6V7I). Oxygen is shown in red, nitrogen in blue, sulfur in yellow, and boron in pink. Hydrogen bonds are shown as dashed lines. Water molecules are shown as red spheres. B, structure of KPC-44 (light green) in complex with vaborbactam (orange). C, superimposed structures of KPC-2 and KPC-44 with bound vaborbactam. For clarity, hydrogen bonds are not shown. D, structure of the active site of KPC-44 apo-enzyme (tan). E, structure alignment of KPC-44 apo-enzyme with the KPC-44 complex with vaborbactam. KPC, *Klebsiella pneumoniae* carbapenemase; PDB, Protein Data Bank.

thiophene ring of vaborbactam and the side chains of Pro167 and Lys73 (Fig. 7).

A comparison of the KPC-44 and KPC-2 structures in complex with vaborbactam indicates they are highly similar (Fig. 7C). Active-site residues are superimposable and the same interactions as those described above for KPC-44/vaborbactam are present with vaborbactam and KPC-2. This is consistent with the similar  $k_2$  values for vaborbactam with KPC-2 and KPC-44 (Table 3).

Superposition of the structure of the KPC-44/vaborbactam complex with that of the KPC-44 apo protein revealed that vaborbactam binding in the active site of KPC-44 protein induces changes in the conformation of residue Trp105 (Fig. 7, D and E). The change observed with Trp105 could be due to the formation of hydrophobic interactions as described above. In addition, similar to AVI, the binding of vaborbactam in the active site of KPC-44 enzyme also causes further disorder in the 270-loop so that residues Lys270-Asn284 cannot be modeled. This suggests communication between the active site and the 270-loop in vaborbactam binding that could be related to the 4-fold lower  $k_2/K_i$  value for KPC-44 than KPC-2.

## Discussion

Although bacteria producing the KPC-2 or KPC-3 carbapenemases are resistant to nearly all of the  $\beta$ -lactam antibiotics, CAZ-AVI combination therapy has been successful in treating these infections. However, prolonged treatment of patients colonized with KPC-2- or KPC-3-producing *K. pneumoniae* strains with CAZ-AVI has resulted in CAZ-AVI resistant strains. *bla*<sub>KPC</sub> genotyping combined with heterologous expression experiments confirmed that while some cases of the CAZ-AVI resistance phenotype are due to amino acid substitutions D179Y and D179Y/T243M in the KPC-2 or KPC-3 enzymes to yield KPC-31 (KPC-3 D179Y), KPC-32 (KPC-2 D179Y/T243M), and KPC-33 (KPC-2 D179Y), others are attributed to amino acid deletions ( $\Delta$ 242-GT-243) in KPC-2 or KPC-3, which correspond to KPC-14 and KPC-28, respectively (29, 31, 43) (Fig. S1). Further characterization revealed that all of these mutations result in the loss of carbapenem resistance (29, 32, 35–37). These findings are supported by *in vitro* experiments using purified KPC variants, which showed that these variants exhibit negligible carbapenem hydrolysis activity (32, 37). In addition, penicillin

hydrolysis is also abolished in the KPC-2 variants harboring the D179Y mutation (KPC-32 and KPC-33) (32, 37). Therefore, for these KPC variants, gain of CAZ-AVI resistance is concomitant with the loss of carbapenemase and/or penicillinase activity.

KPC-44 is another CAZ-AVI-resistant variant of KPC-2 that occurred after prolonged CAZ-AVI treatment of a patient colonized with KPC-2-producing *K. pneumoniae* (30). In contrast to the variants noted above, KPC-44 evolved from KPC-2 via the duplication of 15 amino acids (Ala262–Glu276) after Glu276 (Fig. S1) (30). More importantly, *K. pneumoniae* isolates producing KPC-44 retain carbapenem resistance, albeit at lower levels than the KPC-2-producing parental strain (30). In this study, we found that KPC-44 confers 4-fold higher CAZ MIC levels and similar ampicillin MIC levels to the *E. coli* cells than their KPC-2 counterpart (Table 1). Further, kinetic analysis of  $\beta$ -lactam hydrolysis with purified KPC enzymes revealed that KPC-44 exhibited 4-fold higher CAZ hydrolysis levels and similar ampicillin hydrolysis levels than the KPC-2 enzyme (Table 2). In addition, KPC-44 retains the ability to hydrolyze imipenem and meropenem, although not as efficiently as the KPC-2 enzyme (Table 2). Therefore, in contrast to the CAZ-AVI-resistant KPC variants noted above, KPC-44 retains the carbapenemase and penicillinase activity of KPC-2 enzyme.

To understand the structural basis for the catalytic activity of KPC-44, we determined its X-ray crystal structure. Comparison of the KPC-44 structure with that of the KPC-2 enzyme revealed that the insertion of 15 amino acids in KPC-2 resulted in an extended and opened 270-loop (Fig. 3). In addition, the insertion also increased the flexibility of the 270-loop such that the structure of six amino acids (Lys270–Ser275) on the loop could not be modeled (Fig. 3C). Besides its effect on the conformation of 270-loop, the insertion also causes the movement of the 240-loop toward the active site through altered interactions between the 240- and 270-loops (Figs. 3 and 5). Interestingly, we previously showed that KPC variants with amino acid changes on either 240-loop or 270-loop such as KPC-3 (KPC-2 H274Y) and KPC-6 (KPC-2 V240G) display significantly higher catalytic efficiency for CAZ hydrolysis than the KPC-2 enzyme (13). In addition, combination of amino acid substitutions from both the 240- and 270-loops (KPC-8, V240G/H274Y; KPC-9, KPC-2 V240A/H274Y) additively increases the catalytic efficiency for CAZ hydrolysis, when compared with the effect of single amino acid substitutions (13). While the H274Y substitution is proposed to form an additional hydrogen bond between the hydroxyl side chain of tyrosine and the amine of the aminothiazole ring of CAZ, the V240A/G substitution reduces steric hindrance to better accommodate CAZ (13, 41).

The structure of a deacylation deficient mutant (E166Q) of KPC-2 was recently determined in complex with the CAZ acyl-enzyme intermediate, revealing that the active-site omega loop was disordered to accommodate CAZ. The structure also showed movement of the 240-loop and residues Lys270–His274 on the 270-loop were disordered (41). This suggests structural changes in the omega, 240-loop and 270-loop may be connected, that is, that interactions with the omega loop stabilize

the 240-loop and the 270-loop and vice versa. By this view, the duplication in the 270-loop in KPC-44 results in fewer contacts and a change in conformation of the 240-loop, which could destabilize the omega loop and more readily allow an open conformation to accommodate CAZ. Consistent with this hypothesis, MD simulations show a larger overall RMSD, and the SD of the distances between Ser70 and Glu166 as well as Asn170 during the simulation is larger for KPC-44 than KPC-2.

AVI inhibits SBLs including KPC-2 enzyme by forming a reversible covalent bond between C7 of AVI and the hydroxyl group of the catalytic Ser70 of  $\beta$ -lactamases through an acylation reaction (Fig. 2B) (16, 17, 21). The reaction follows a two-step mechanism that includes binding and carbamylation (16). Therefore, the carbamylation efficiency ( $k_2/K_i$ ) is an important factor in determining the sensitivity of SBLs to inhibition by AVI. Determination of the effect of D179Y on  $k_2/K_i$  for AVI with KPC-2 and KPC-3 by two independent studies obtained very different results in that the D179Y substitution greatly decreases the AVI  $k_2/K_i$  for the KPC-2 enzyme but barely affects the AVI  $k_2/K_i$  for the KPC-3 enzyme although the KPC-2 and KPC-3 enzymes display similar AVI  $k_2/K_i$  (28, 32). This variation is most likely attributed to very low activity of D179Y mutant of the KPC-2 and KPC-3 enzymes in hydrolyzing the chromogenic cephalosporins nitrocefin and CENTA, which were used as the reporter substrate for the measurement of the AVI  $k_2/K_i$  (28, 32). In contrast, KPC-44 retains significant activity in hydrolyzing nitrocefin, although lower than that of the KPC-2 enzyme (Table 2). Determination of the AVI carbamylation efficiency using nitrocefin as the reporter substrate revealed that the KPC-44 enzyme exhibits a 12-fold lower  $k_2/K_i$  for AVI than the KPC-2 enzyme (Table 3). In contrast, the AVI decarbamylation rate is similar for the KPC-2 and KPC-44 enzymes (Table 3). Therefore, the decreased AVI susceptibility observed with KPC-44 is attributed to lower AVI carbamylation efficiency than the KPC-2 enzyme.

In order to understand the structural basis for AVI resistance observed with KPC-44, the structure of KPC-44 in covalent complex with AVI was determined. Comparison of the structure of the complex with the apo structure of KPC-44 revealed that the 270-loop was more disordered in the complex structure with residues Lys270–Asn284 unmodeled. This suggests that the extended 270-loop of KPC-44, which borders the active site of the enzyme, may interfere with binding and/or carbamylation of AVI in the active site of KPC-44 and is thus dislocated after AVI carbamylation. In addition, the KPC-44/AVI structure displays an alternative conformation of the Cys69–Cys238 disulfide bond compared to the KPC-44 apo-enzyme. However, the altered conformation of the disulfide bond is not observed with KPC-2 after AVI acylation although AVI adopts very similar conformation in the active site of KPC-2 and KPC-44 enzymes (Fig. 4F). This suggests that the conformation of the disulfide bond in KPC-44 may not favor AVI binding and/or acylation and thus its rearrangement is required for the process. As Cys238 is located on the 240-loop that adopts different conformations between KPC-2 and KPC-44 enzymes, this further suggests that the 240-loop of the KPC-2 enzyme may be in a conformation for efficient binding



## Structure and mechanism of KPC-44 carbapenemase variant

and/or carbamylation of AVI. Therefore, the altered conformation of the 240- and 270-loops may contribute to the reduced  $k_2/K_i$  for AVI.

Besides treating infections caused by KPC-producing pathogens, CAZ-AVI has also been used for treating infections caused by bacterial pathogens expressing other SBLs such as CTX-M-type extended-spectrum  $\beta$ -lactamases and some class D  $\beta$ -lactamases such as the OXA-48 carbapenemase. Unsurprisingly, there is also the occurrence of CAZ-AVI resistant CTX-M-14 variants in the clinic, which are due to amino acid substitutions (44). In addition, although there are no reports of CAZ-AVI-resistant variants of OXA-48 in natural isolates, they can be selected *in vitro* (45). However, the *in vitro* selected OXA-48 variants lost penicillinase and carbapenemase activity, as found for AVI resistant KPC variants other than KPC-44. This indicates that penicillins and carbapenems are still a viable option to treat infections related to these variants. Nevertheless, the combination of CAZ-AVI resistance and broad substrate profile of KPC-44 variant limit the treatment options for KPC-44-producing pathogens.

Finally, vaborbactam is a cyclic boronic acid-based  $\beta$ -lactamase inhibitor that has a broad spectrum of activity against class A and C  $\beta$ -lactamases (39, 46). Its combination with meropenem (Vabomere) was recently approved by the Food and Drug Administration to treat complicated urinary tract infections (47). Determination of vaborbactam sensitivity of KPC-44 in this study revealed that KPC-44 has similar sensitivity as KPC-2 to this inhibitor. Therefore, meropenem/vaborbactam combination therapy can still be an option in treating KPC-44-associated infections.

## Experimental procedures

### Bacterial strains and plasmids

*E. coli* XL-1 Blue was used as the host for molecular cloning and *E. coli* Top10 was used as the host for determination of  $\beta$ -lactam antibiotic MICs provided by the KPC-2 and KPC-44 enzymes. For this work, the *bla*<sub>KPC-2</sub> gene encoding the entire sequence of the KPC-2 enzyme was cloned onto the pTP123 plasmid, on which the expression of KPC-2 enzyme is under the control of an IPTG-inducible *trc* promoter (13). The KPC-2-pTP123 plasmid was used as the template for the construction of KPC-44-pTP123 plasmid using site-directed mutagenesis with the forward primer (5'-CGCCTAACAA GGATGACAAGCACAGCGAGGCCGTCATCGCCGCTGC GGCTAGAC- 3') and the reverse primer (5' -CTGTGC TTGTCATCCTTGTAGGCGCCCGGTGTAGACGGCC TCGCTGTGCTTG- 3').

The *E. coli* SHuffle strain (New England Biolabs), which is engineered to overexpress proteins containing disulfide bonds in cytoplasm (48), was used as the host for the overexpression of KPC-2 and KPC-44 in the cytoplasm. For this purpose, the DNA encoding KPC-2 and KPC-44 without the signal sequence (N-terminal 25 amino acids) was amplified from the KPC-2-pTP123 and KPC-44-pTP123 plasmids, respectively, endonuclease-restricted and inserted between *Nde* I and *Eco*R I restriction sites of pET28a-Tobacco Etch Virus (TEV), which

is a modified pET28a vector with a TEV protease recognition sequence inserted between the 6×His tag and the protein of interest. The sequences of the recombinant plasmid KPC-2-pET28a-TEV and KPC-44-pET28a-TEV were confirmed with DNA sequencing.

As described previously, crystallization of the KPC-2 enzyme can be facilitated by removing the last four residues of the protein (49, 50). Therefore, KPC-44 without the last four amino acids (KPC-44  $\Delta$ 4) was used for crystallization. For this purpose, the DNA encoding KPC-44  $\Delta$ 4 was inserted between *Nde* I and *Eco*R I restriction sites of pET28a-TEV to create KPC-44  $\Delta$ 4-pET28a-TEV. The sequence of the recombinant plasmid was confirmed by DNA sequencing.

### Determination of antibiotic resistance levels

The  $\beta$ -lactam MICs for *E. coli* encoding KPC-2 or KPC-44 were determined using the broth dilution method as described previously (51, 52). Briefly, overnight cultures of *E. coli* Top10 cells expressing KPC-2 or KPC-44 were diluted 1:10,000 in 2×YT broth containing 12.5  $\mu$ g ml<sup>-1</sup> chloramphenicol. Then, 190  $\mu$ l of diluted culture was added to the wells of a 96-well plate that contained 10  $\mu$ l of appropriate concentrations of ampicillin or CAZ. The plates were incubated with shaking at 37 °C for 16 h before the  $A_{600}$  of the cultures were recorded. The antibiotic resistance levels of the bacterial strains were recorded as the MIC of the antibiotic, which was defined as the lowest concentration of the antibiotic that can inhibit 90% of the  $A_{600}$ , compared with that of the cultures without  $\beta$ -lactam antibiotics. Resistance levels of imipenem and meropenem were determined using the same method as that for ampicillin and CAZ except that the overnight cultures of the recombinant *E. coli* Top10 cells were 1:1000 diluted in 2×YT broth containing 12.5  $\mu$ g ml<sup>-1</sup> chloramphenicol before mixing with imipenem or meropenem. The resistance levels for CAZ-AVI were tested at a constant AVI concentration of 4  $\mu$ g ml<sup>-1</sup> with increasing concentrations of CAZ, and the MIC values represent the lowest concentration of CAZ that can inhibit 90% increase of  $A_{600}$  (31, 32, 34). MIC measurements were repeated three times and the results were consistent across replicates.

### Expression and purification of KPC-2 WT and mutants

For the overexpression of KPC-2, KPC-44, and KPC-44  $\Delta$ 4 proteins, the corresponding plasmid was transformed into *E. coli* SHuffle cells. A few well-isolated colonies were inoculated in LB broth containing 25  $\mu$ g ml<sup>-1</sup> kanamycin and incubated overnight at 30 °C with vigorous shaking. Overnight cultures were 1:100 diluted in 1.5 L of LB broth containing 25  $\mu$ g ml<sup>-1</sup> kanamycin and incubated at 30 °C with vigorous shaking until the  $A_{600}$  reached 0.8 at which point IPTG was added to a final concentration of 0.5 mM. Incubation with shaking was continued at 18 °C for 16 h before cells were pelleted by centrifugation at 4000 rpm for 20 min.

For the purification of 6×His-tagged KPC-2 protein, the cell pellet was resuspended in lysis buffer (20 mM Hepes, pH 7.4, 500 mM NaCl, 20 mM imidazole). Cells were lysed using a

French Press homogenizer and the released genomic DNA was broken down by a short period of sonication. The cell debris was removed by centrifugation at 12,000g for 30 min, and the soluble fraction of the lysate was filtered with a 0.45 µm filter unit and loaded onto a 5 ml HisTrap FF column (GE Healthcare). After washing the column with lysis buffer, 6×His-tagged recombinant KPC-2 protein was eluted with a 20 to 500 mM imidazole gradient in the Lysis Buffer. Fractions containing the recombinant proteins were pooled and concentrated and buffer exchanged to the lysis buffer with a 10-kDa cut-off Amicon concentrator unit (EMD Millipore). The 6×His tag was removed by incubation overnight at 4 °C with TEV protease at 1: 50 (TEV: His-KPC-2) ratio, and the TEV protease was removed by incubation with Ni Sepharose Fast Flow beads (GE Healthcare). KPC-2 protein was further purified by gel-filtration chromatography with a Superdex 75 Increase (10/300) column (GE Healthcare) using 20 mM Hepes, pH 7.4, 150 mM NaCl as the running buffer. Fractions containing the recombinant proteins were pooled and concentrated with a 10-kDa cut-off Amicon concentrator unit (EMD Millipore). The KPC-44 and KPC-44 Δ4 proteins were purified using the same procedure as that for KPC-2. The purity of each protein was over 95% based on SDS-PAGE analysis. Protein concentrations were determined by measuring the absorbance at 280 nm with a DU800 spectrophotometer (Beckman Coulter) using an extinction coefficient of 39,545 M<sup>-1</sup> cm<sup>-1</sup> for KPC-2 and 41,035 M<sup>-1</sup> cm<sup>-1</sup> for KPC-44 and KPC-44 Δ4, respectively.

#### Kinetic analysis of β-lactam hydrolysis by KPC-2 and KPC-44 enzyme

Enzyme kinetic parameters for the hydrolysis of ampicillin, CAZ, cefotaxime, nitrocefin, imipenem, and meropenem by the KPC-2 and KPC-44 enzymes were determined at 30 °C in 50 mM sodium phosphate buffer, pH 7. Bovine serum albumin (BSA) was included in the buffers at the final concentration of 1 µg ml<sup>-1</sup> to stabilize the enzymes and prevent absorption to the cuvette.

Antibiotic hydrolysis was monitored with a DU800 spectrophotometer (Beckman Coulter) equipped with a thermostatically controlled cell by following the absorbance change of ampicillin at 235 nm ( $\Delta\epsilon_{235\text{nm}} = -900 \text{ M}^{-1} \text{ cm}^{-1}$ ), CAZ at 260 nm ( $\Delta\epsilon_{260\text{nm}} = -10,500 \text{ M}^{-1} \text{ cm}^{-1}$ ), cefotaxime at 260 nm ( $\Delta\epsilon_{260\text{nm}} = -7250 \text{ M}^{-1} \text{ cm}^{-1}$ ), nitrocefin at 482 nm ( $\Delta\epsilon_{482\text{nm}} = 15,000 \text{ M}^{-1} \text{ cm}^{-1}$ ), imipenem at 300 nm ( $\Delta\epsilon_{300\text{nm}} = -9000 \text{ M}^{-1} \text{ cm}^{-1}$ ), and meropenem at 300 nm ( $\Delta\epsilon_{300\text{nm}} = -8416 \text{ M}^{-1} \text{ cm}^{-1}$ ).  $k_{\text{cat}}$  and  $K_m$  parameters were determined under initial-rate conditions by fitting the initial velocity ( $v_o$ ) at various substrate concentrations to the Michaelis–Menten equation ( $v = V_{\text{max}} [S]/(K_m + [S])$ ) using GraphPad Prism 5 ([www.graphpad.com](http://www.graphpad.com)). When  $V_{\text{max}}$  could not be determined because  $K_m$  was too high, the  $k_{\text{cat}}/K_m$  value was determined by analyzing the complete hydrolysis time courses at low antibiotic concentration and fitting the data to the equation  $v = k_{\text{cat}}/K_m [E][S]$ , where  $[S] \ll K_m$ . Kinetic

parameters were averaged from at least two independent determinations.

#### Determination of AVI, clavulanate, and vaborbactam inhibition potency for KPC-2 and KPC-44

The sensitivity of KPC enzymes to inhibition by AVI, clavulanate, and vaborbactam was determined using purified KPC-2 or KPC-44 enzymes. A total of 2 nM of KPC-2 and 4 nM of KPC-44 was mixed with inhibitors at varying concentrations in 50 mM sodium phosphate (pH 7) containing 0.02% Tween-20 and 2 µg/ml BSA and incubated at room temperature for 10 min (clavulanate), 20 min (AVI), or 1 h (vaborbactam). The reaction was initiated upon the addition of the same volume of 30 µM nitrocefin prepared in 50 mM sodium phosphate (pH 7) containing 0.02% Tween-20. The initial velocity ( $v_o$ ) of nitrocefin hydrolysis in the assays with inhibitors was expressed as the percentage of  $v_o$  of the reactions without inhibitors, which was set as 100%. IC<sub>50</sub> of inhibitors were obtained by plotting  $v_o$  versus logarithms of inhibitor concentrations (Log[I]) and fitting the data log(inhibitor) versus normalized response using GraphPad Prism5 ([www.graphpad.com](http://www.graphpad.com)).

#### Determination of AVI carbamylation efficiency ( $k_2/K_i$ ) and decarbamylation rate ( $k_{-2}$ ) for the KPC-2 and KPC-44 enzymes

AVI carbamylation experiments were carried out at 30 °C in 50 mM sodium phosphate (pH 7) containing 0.02% Tween-20 and 1 µg/ml BSA using a Tecan Infinite M Plex microplate reader with 200 µM nitrocefin as the substrate. A total of 1 nM KPC-2 and 2 nM KPC-44 enzyme were used, respectively. AVI was tested up to 20 µM for KPC-2 and 100 µM for KPC-44, respectively.

Nitrocefin hydrolysis data were fit to the following two-step, reversible equation model  $E + I \rightleftharpoons EI \rightleftharpoons EI^*$ , where  $k_1$  and  $k_{-1}$  describe the formation and dissociation EI from E + I,  $k_2$  and  $k_{-2}$  describe formation and reversion of EI\* from EI and where  $K_i = \frac{k_{-1}}{k_1}$ , as described previously (16, 17). Progress curves of nitrocefin hydrolysis were fit to Equation 1 to obtain the pseudo first-order constant  $k_{\text{obs}}$ .

$$P = V_s t + (V_o - V_s) \frac{(1 - e^{-kt})}{k} \quad (1)$$

In the equation,  $V_o$  represents the uninhibited enzyme velocity that is measured in a reaction with KPC enzyme and no AVI, whereas  $V_s$  represents fully inhibited enzyme velocity that is measured in a reaction without any enzyme.  $k_{\text{obs}}$  obtained with varying AVI concentrations was then fit to Equation 2 to derive AVI acylation efficiency ( $k_2/K_i$ ) for the KPC-2 and KPC-44 enzymes.

$$k_{\text{obs}} = k_{-2} + \frac{k_2}{K_i} \frac{[I]}{\left(1 + \frac{[S]}{K_m}\right)} \quad (2)$$

The rate of AVI decarbamylation ( $k_{-2}$ ) from carbamylated KPC enzymes was determined at 30 °C using a jump dilution

## Structure and mechanism of KPC-44 carbapenemase variant

method, followed with a continuous assay to monitor regain of activity, as described previously (18). A total of 1  $\mu\text{M}$  KPC-2 or 2  $\mu\text{M}$  KPC-2 was incubated with 10  $\mu\text{M}$  or 20  $\mu\text{M}$  AVI in 50 mM sodium phosphate (pH 7) containing 0.02% Tween-20 at room temperature for 2 h to inactivate the KPC enzyme. The inactivation mixture was then diluted by 100-fold into 50 mM sodium phosphate (pH 7) containing 0.02% Tween-20 and 20  $\mu\text{l}$  of the diluted inactivation mixture was added to 180  $\mu\text{l}$  of 200  $\mu\text{M}$  nitrocefin. Absorbance at 482 nm ( $A_{482}$ ) was continuously recorded in a Tecan Infinite M Plex microplate reader with the temperature set at 30 °C. Data were fit to Equation 1 to obtain  $k_2$ , where  $V_0$  represents fully inhibited enzyme velocity and  $V_s$  represents the uninhibited enzyme velocity. Vaborbactam borylation efficiency ( $k_2/K_i$ ) and deborylation rate ( $k_{-2}$ ) for KPC-2 and KPC-44 enzymes were determined using the same methods as those for AVI.

### X-ray structure determination of KPC-44

KPC-44  $\Delta 4$  was purified to homogeneity and concentrated to 30 mg  $\text{ml}^{-1}$ . Crystallization screening was performed using PEG/Ion Screen (Hampton Research), PEGs Suite (NeXtal Biotechnologies), JCSG Core I Suite (NeXtal Biotechnologies), JCSG Core IV Suite (NeXtal Biotechnologies), and MPD Suite (NeXtal Biotechnologies). A total of 0.2  $\mu\text{l}$  of protein solutions (15 or 30 mg  $\text{ml}^{-1}$ ) in 50 mM Hepes (pH 7.4), 150 mM NaCl were mixed with 0.2  $\mu\text{l}$  of reservoir solution by using a Mosquito automated nanoliter liquid handler robot (TTP Lab-Tech). The mixture was allowed to equilibrate against the reservoir solution (70  $\mu\text{l}$ ) at 25 °C by using the hanging-drop method. Crystals formed after 2 months for 30 mg  $\text{ml}^{-1}$  KPC-44  $\Delta 4$  only with reservoir solutions containing 0.2 M lithium sulfate, 0.1 M phosphate-citrate, pH 4.2, and 20% (w/v) PEG 1000 (H7 of JSCG Core I suite). Therefore, the crystallization condition for KPC-44  $\Delta 4$  protein was further optimized by varying the concentration of KPC-44  $\Delta 4$  protein (20–50 mg  $\text{ml}^{-1}$ ), the pH of 0.1 M phosphate-citrate (pH 3.8–4.8) and the concentration of PEG 1000 (18–24% (w/v)) of the reservoir solutions. After optimization, diffraction quality crystals formed within a few days for 40 to 50 mg  $\text{ml}^{-1}$  protein with reservoir solutions containing 0.2 M lithium sulfate, 0.1 M phosphate-citrate, pH 4 to 4.4, and 22 to 24% (w/v) PEG 1000. For data collection, crystals of KPC-44  $\Delta 4$  were either directly flash-frozen in liquid nitrogen or soaked in cryoprotectant solution (20% ethylene glycerol, 20% glycerol, or 20% 2-methyl-2, 4-pentanediol (diluted in reservoir solution) for 30 s before being flash frozen in liquid nitrogen. In addition, the crystals of KPC-44  $\Delta 4$  were also soaked for different periods of time (from 10 s to 4 h) with 10 mM AVI or 5 mM vaborbactam that was prepared in the reservoir solution containing 20% ethylene glycerol before being frozen in liquid nitrogen. Diffraction data were collected on the 8.2.1 or 5.0.3 beamline at the Advanced Light Source synchrotron in Berkeley.

Diffraction data for the KPC-44  $\Delta 4$  apoenzyme and in complex with AVI or vaborbactam were indexed, integrated, and scaled using iMosflm and Scala in the CCP4i (53, 54). The structures were solved by molecular replacement using the

program Phaser with the truncated KPC-2 structure (KPC-2  $\Delta 4$ ) (PDB ID: 3C5A) as the initial search model. The structures of KPC-44  $\Delta 4$  apo protein, KPC-44  $\Delta 4$  apo protein without cryoprotectant, KPC-44  $\Delta 4$ /AVI, and KPC-44  $\Delta 4$ /vaborbactam were solved to 1.26 Å, 1.31 Å, 1.37 Å, and 1.70 Å, respectively. The structures were further refined using PHENIX with at least ten rounds of manual remodeling in COOT between refinement cycles (55, 56). AVI and vaborbactam were manually built into the protein structure in Coot. The geometry restraints were calculated using the Grade Web Server (<http://grade.globalphasing.org>) and the mFo- $F_c$  omit map was generated in PHENIX (55). AVI and vaborbactam occupancy was manually assigned based upon inspection of electron density and subsequently refined in Phenix with at least ten rounds of refinement (55). The fully refined structures are deposited in the Protein Data Bank (PDB) with the entry codes 8TJM (KPC-44), 8TN0 (KPC-44 w/o cryoprotectant), 8TMR (KPC-44/AVI), and 8TMT (KPC-44/vaborbactam). Statistics for data collection and refinement are found in Table S1. All structure figures were generated using the UCSF Chimera program (57).

### Modeling and MD simulations

The initial coordinates for KPC-2 enzyme simulations come from the crystal structures downloaded from PDB entry 2OV5 (58), while those of KPC-44 were directly from this work. The missing loop Asn269-Glu276 in KPC-44 crystal structure was built using the loop\_modelling\_notmove.py script from Modeller 10.1 (59). Protein Preparation Workflow from Maestro (Schrödinger LLC) was then used for pdb file clean-up, adding hydrogen, assigning protonation states (assuming a pH of 7.4 for the ionizable groups), and removing side chain ambiguity.

GROMACS version 2020.7 and CHARMM36-feb2021 forcefield were used for MD simulations. For each initial set of coordinates, the periodic boundary condition was applied as follows: the box was set as cubic with absolute size of each side greater than the largest dimension of the system by 10 Å. Explicit water was added, and the system charge was neutralized with 150 mM sodium and chloride ions. A steepest descent energy minimization was performed to remove steric clashes or inappropriate geometry until the structure converged. Consecutive 100 ps NVT ensemble simulation with T at 300 K using V-rescale and 100 ps NPT ensemble simulations with T at 300 K and pressure at 1 bar with Berendsen barostat were then performed to allow temperature and pressure coupling for protein and nonprotein groups. The convergence of system temperature, pressure, and density were confirmed. Finally, the production run of 100 ns was performed. Short range van der Waals was calculated using Verlet neighbor searching algorithm with a cut-off of 1.2 nm. Coulomb was calculated using Particle Mesh Ewald and the cut-off was set as 1.2 nm. During the production run, coordinate frames were saved at every 10 ps. Three 100 ns replicates were performed for each protein. The trajectories were visualized through the following gmx trjconv commands: whole – center – mol(compact) – rot+trans. The



postsimulation distance and RMSD analysis after each run were performed by calling respective commands built in GROMACS. The MD simulation was performed on Longhorn server from Texas Advanced Computing Center under project CHE21040. The GROMACS was compiled with GPU-enabled code and the job was mainly run on GPU.

## Data availability

Accession codes: Coordinates and structure factors have been deposited in the Protein Data Bank under accession codes KPC-44, 8TJM; KPC-44 w/o cryoprotectant, 8TN0; KPC-44-avibactam, 8TMR; KPC-44-vaborbactam, 8TMT. All relevant data associated with the paper are available upon request from the corresponding author.

**Supporting information**—This article contains supporting information.

**Acknowledgments**—The ALS-ENABLE beamlines are supported in part by the National Institutes of Health, National Institute of General Medical Sciences, grant P30 GM124169-01. The Advanced Light Source is a Department of Energy Office of Science User Facility under Contract No. DE-AC02-05CH11231.

**Author contributions**—Z. S., H. L., L. H., N. N., and B. S. investigation; Z. S., H. L., L. H., N. N., and B. S. methodology; Z. S., H. L., L. H., N. N., B. S., B. V. V. P., and T. P. formal analysis; Z. S. and T. P. conceptualization; Z. S. data curation; Z. S. writing—original draft; H. L., L. H., B. S., J. W., B. V. V. P., and T. P. writing—review and editing; J. W., B. V. V. P., and T. P. supervision; J. W. resources; B. V. V. P. and T. P. funding acquisition.

**Funding and additional information**—This work was funded by NIH grant AI32956 to T. P. and Welch Foundation grant Q1279 to B. V. V. P. The content is solely the responsibility of the authors and does not necessarily represent the official views of the National Institutes of Health.

**Conflict of interest**—The authors declare that they have no conflicts of interest with the contents of this article.

**Abbreviations**—The abbreviations used are: BSA, bovine serum albumin; CAZ-AVI, ceftazidime/avibactam; KPC, *Klebsiella pneumoniae* carbapenemase; MD, molecular dynamics; MIC, minimum inhibitory concentration; PDB, Protein Data Bank; SBL, serine  $\beta$ -lactamase; TEV, Tobacco Etch Virus.

## References

- Livermore, D. M., and Woodford, N. (2006) The  $\beta$ -lactamase threat in enterobacteriaceae, *Pseudomonas* and *acinetobacter*. *Trends Microbiol.* **14**, 413–420
- Lovering, A. L., Safadi, S. S., and Strynadka, N. C. J. (2012) Structural perspective of peptidoglycan biosynthesis and assembly. *Annu. Rev. Biochem.* **81**, 451–478
- Fisher, J. F., Meroueh, S. O., and Mobashery, S. (2005) Bacterial resistance to  $\beta$ -lactam antibiotics: compelling opportunism, compelling opportunity. *Chem. Rev.* **105**, 395–424
- Palzkill, T. (2018) Structural and mechanistic basis for extended-spectrum drug-resistance mutations in altering the specificity of TEM, CTX-M, and KPC  $\beta$ -lactamases. *Front. Mol. Biosci.* **5**, 16
- Strynadka, N. C. J., Adachi, H., Jensen, S. E., Johns, K., Sielecki, A., Betzel, C., *et al.* (1992) Molecular structure of the acyl-enzyme intermediate in  $\beta$ -lactam hydrolysis at 1.7 Å resolution. *Nature* **359**, 700–705
- Fisher, J., and Mobashery, S. (2009) Three decades of the class A  $\beta$ -lactamase acyl-enzyme. *Curr. Protein Pept. Sci.* **10**, 401–407
- Meroueh, S. O., Fisher, J. F., Schlegel, H. B., and Mobashery, S. (2005) *Ab Initio* QM/MM study of class A  $\beta$ -lactamase acylation: dual participation of Glu166 and Lys73 in a concerted base promotion of Ser70. *J. Am. Chem. Soc.* **127**, 15397–15407
- Adachi, H., Ohta, T., and Matsuzawa, H. (1991) Site-directed mutants, at position 166, of RTEM-1 beta-lactamase that form a stable acyl-enzyme intermediate with penicillin. *J. Biol. Chem.* **266**, 3186–3191
- Yigit, H., Queenan, A. M., Anderson, G. J., Domenech-Sanchez, A., Biddle, J. W., Steward, C. D., *et al.* (2001) Novel carbapenem-hydrolyzing  $\beta$ -lactamase, KPC-1, from a carbapenem-resistant strain of *Klebsiella pneumoniae*. *Antimicrob. Agents Chemother.* **45**, 11
- Bratu, S., Brooks, S., Burney, S., Kochar, S., Gupta, J., Landman, D., *et al.* (2007) Detection and spread of *Escherichia coli* possessing the plasmid-borne carbapenemase KPC-2 in brooklyn, New York. *Clin. Infect. Dis.* **44**, 972–975
- Hagemann, J. B., Pfennigwerth, N., Gattermann, S. G., von Baum, H., and Essig, A. (2018) KPC-2 carbapenemase-producing *Pseudomonas aeruginosa* reaching Germany. *J. Antimicrob. Chemother.* **73**, 1812–1814
- Martinez, T., Martinez, I., Vazquez, G. J., Aquino, E. E., and Robledo, I. E. (2016) Genetic environment of the KPC gene in *Acinetobacter baumannii* ST2 clone from Puerto Rico and genomic insights into its drug resistance. *J. Med. Microbiol.* **65**, 784–792
- Mehta, S. C., Rice, K., and Palzkill, T. (2015) Natural variants of the KPC-2 carbapenemase have evolved increased catalytic efficiency for ceftazidime hydrolysis at the cost of enzyme stability. *PLoS Pathog.* **11**, e1004949
- Bush, K., and Bradford, P. A. (2019) Interplay between  $\beta$ -lactamases and new  $\beta$ -lactamase inhibitors. *Nat. Rev. Microbiol.* **17**, 295–306
- Papp-Wallace, K. M., Bethel, C. R., Distler, A. M., Kasuboski, C., Taracila, M., and Bonomo, R. A. (2010) Inhibitor resistance in the KPC-2  $\beta$ -lactamase, a preeminent property of this class A  $\beta$ -lactamase. *Antimicrob. Agents Chemother.* **54**, 890–897
- Ehmann, D. E., Jahic, H., Ross, P. L., Gu, R.-F., Hu, J., Kern, G., *et al.* (2012) Avibactam is a covalent, reversible, non- $\beta$ -lactamase inhibitor. *Proc. Natl. Acad. Sci. U. S. A.* **109**, 11663–11668
- Ehmann, D. E., Jahic, H., Ross, P. L., Gu, R.-F., Hu, J., Durand-Réville, T. F., *et al.* (2013) Kinetics of avibactam inhibition against class A, C, and D  $\beta$ -lactamases. *J. Biol. Chem.* **288**, 27960–27971
- Dubreuil, L. J., Mahieux, S., Neut, C., Miossec, C., and Pace, J. (2012) Anti-anaerobic activity of a new  $\beta$ -lactamase inhibitor NXL104 in combination with  $\beta$ -lactams and metronidazole. *Int. J. Antimicrob. Agents* **39**, 500–504
- Levasseur, P., Girard, A.-M., Claudon, M., Goossens, H., Black, M. T., Coleman, K., *et al.* (2012) *In vitro* antibacterial activity of the ceftazidime-avibactam (NXL104) combination against *Pseudomonas aeruginosa* clinical isolates. *Antimicrob. Agents Chemother.* **56**, 1606–1608
- Aktaş, Z., Kayacan, C., and Oncul, O. (2012) *In vitro* activity of avibactam (NXL104) in combination with  $\beta$ -lactams against Gram-negative bacteria, including OXA-48  $\beta$ -lactamase-producing *Klebsiella pneumoniae*. *Int. J. Antimicrob. Agents* **39**, 86–89
- King, D. T., King, A. M., Lal, S. M., Wright, G. D., and Strynadka, N. C. J. (2015) Molecular mechanism of avibactam-mediated  $\beta$ -lactamase inhibition. *ACS Infect. Dis.* **1**, 175–184
- Pemberton, O. A., Noor, R. E., Kumar, M. V., Sanishvili, R., Kemp, M. T., Kearns, F. L., *et al.* (2020) Mechanism of proton transfer in class A  $\beta$ -lactamase catalysis and inhibition by avibactam. *Proc. Natl. Acad. Sci. U. S. A.* **117**, 5818–5825
- Krishnan, N. P., Nguyen, N. Q., Papp-Wallace, K. M., Bonomo, R. A., and van den Akker, F. (2015) Inhibition of *Klebsiella*  $\beta$ -lactamases (SHV-1 and KPC-2) by avibactam: a structural study. *PLoS One* **10**, e0136813
- Barber, K. E., Ortwine, J. K., and Akins, R. L. (2016) Ceftazidime/avibactam: who says you can't teach an old drug new tricks? *J. Pharm. Pharm. Sci.* **19**, 448

25. Bush, K. (2018) Game changers: new  $\beta$ -lactamase inhibitor combinations targeting antibiotic resistance in gram-negative bacteria. *ACS Infect. Dis.* **4**, 84–87
26. Shirley, M. (2018) Ceftazidime-avibactam: a review in the treatment of serious gram-negative bacterial infections. *Drugs* **78**, 675–692
27. Bianco, G., Boattini, M., Iannaccone, M., Cavallo, R., and Costa, C. (2020) Bloodstream infection by two subpopulations of *Klebsiella pneumoniae* ST1685 carrying KPC-33 or KPC-14 following ceftazidime/avibactam treatment: considerations regarding acquired heteroresistance and choice of carbapenemase detection assay. *J. Antimicrob. Chemother.* **75**, 3075–3076
28. Shapiro, A. B., Moussa, S. H., Carter, N. M., Gao, N., and Miller, A. A. (2021) Ceftazidime-avibactam resistance mutations V240G, D179Y, and D179Y/T243M in KPC-3  $\beta$ -lactamase do not alter cefpodoxime-ETX1317 susceptibility. *ACS Infect. Dis.* **7**, 79–87
29. Shi, Q., Yin, D., Han, R., Guo, Y., Zheng, Y., Wu, S., et al. (2020) Emergence and recovery of ceftazidime-avibactam resistance in *bla* KPC-33-Harboring *Klebsiella pneumoniae* sequence type 11 isolates in China. *Clin. Infect. Dis.* **71**, S436–S439
30. Räisänen, K., Koivula, I., Ilmavirta, H., Puranen, S., Kallonen, T., Lyytikäinen, O., et al. (2019) Emergence of ceftazidime-avibactam-resistant *klebsiella pneumoniae* during treatment, Finland, December 2018. *Euro Surveill.* **24**, 1900256
31. Göttig, S., Frank, D., Mungo, E., Nolte, A., Hogardt, M., Besier, S., et al. (2019) Emergence of ceftazidime/avibactam resistance in KPC-3-producing *Klebsiella pneumoniae* in vivo. *J. Antimicrob. Chemother.* **74**, 3211–3216
32. Compain, F., and Arthur, M. (2017) Impaired inhibition by avibactam and resistance to the ceftazidime-avibactam combination due to the D<sup>179</sup> Y substitution in the KPC-2  $\beta$ -lactamase. *Antimicrob. Agents Chemother.* **61**, e00451-17
33. Wang, Y., Wang, J., Wang, R., and Cai, Y. (2020) Resistance to ceftazidime-avibactam and underlying mechanisms. *J. Glob. Antimicrob. Resist.* **22**, 18–27
34. Papp-Wallace, K. M., Winkler, M. L., Taracila, M. A., and Bonomo, R. A. (2015) Variants of  $\beta$ -lactamase KPC-2 that are resistant to inhibition by avibactam. *Antimicrob. Agents Chemother.* **59**, 3710–3717
35. Wang, C., Zhao, J., Liu, Z., Sun, A., Sun, L., Li, B., et al. (2021) In vivo selection of imipenem resistance among ceftazidime-avibactam-resistant, imipenem-susceptible *Klebsiella pneumoniae* isolate with KPC-33 carbapenemase. *Front. Microbiol.* **12**, 727946
36. Antonelli, A., Giani, T., Di Pilato, V., Riccobono, E., Perriello, G., Menicacci, A., et al. (2019) KPC-31 expressed in a ceftazidime/avibactam-resistant *Klebsiella pneumoniae* is associated with relevant detection issues. *J. Antimicrob. Chemother.* **74**, 2464–2466
37. Oueslati, S., Iorga, B. I., Tlili, L., Exilie, C., Zavala, A., Dortet, L., et al. (2019) Unravelling ceftazidime/avibactam resistance of KPC-28, a KPC-2 variant lacking carbapenemase activity. *J. Antimicrob. Chemother.* **74**, 2239–2246
38. Barnes, M. D., Winkler, M. L., Taracila, M. A., Page, M. G., Desarbre, E., Kreiswirth, B. N., et al. (2017) *Klebsiella pneumoniae* carbapenemase-2 (KPC-2), substitutions at ambler position Asp179, and resistance to ceftazidime-avibactam: unique antibiotic-resistant phenotypes emerge from  $\beta$ -lactamase protein engineering. *mBio* **8**, e00528-17
39. Tsvikovski, R., and Lomovskaya, O. (2020) Biochemical activity of vaborbactam. *Antimicrob. Agents Chemother.* **64**, e01935-19
40. Tsvikovski, R., and Lomovskaya, O. (2020) Potency of vaborbactam is less affected than that of avibactam in strains producing KPC-2 mutations that confer resistance to ceftazidime-avibactam. *Antimicrob. Agents Chemother.* **64**, e01936-19
41. Tooke, C. L., Hinchliffe, P., Bonomo, R. A., Schofield, C. J., Mulholland, A. J., and Spencer, J. (2021) Natural variants modify *Klebsiella pneumoniae* carbapenemase (KPC) acyl-enzyme conformational dynamics to extend antibiotic resistance. *J. Biol. Chem.* **296**, 100126
42. Alsenani, T. A., Viviani, S. L., Kumar, V., Taracila, M. A., Bethel, C. R., Barnes, M. D., et al. (2022) Structural characterization of the D179N and D179Y variants of KPC-2  $\beta$ -lactamase:  $\Omega$ -loop destabilization as a mechanism of resistance to ceftazidime-avibactam. *Antimicrob. Agents Chemother.* **66**, e02414–e02421
43. Beyrouthy, R., Robin, F., Lessene, A., Lacomat, I., Dortet, L., Naas, T., et al. (2017) MCR-1 and OXA-48 in vivo acquisition in KPC-producing *Escherichia coli* after colistin treatment. *Antimicrob. Agents Chemother.* **61**, e02540-16
44. Both, A., Büttner, H., Huang, J., Perbandt, M., Belmar Campos, C., Christner, M., et al. (2017) Emergence of ceftazidime/avibactam non-susceptibility in an MDR *Klebsiella pneumoniae* isolate. *J. Antimicrob. Chemother.* **72**, 2483–2488
45. Fröhlich, C., Sørum, V., Thomassen, A. M., Johnsen, P. J., Leiros, H.-K. S., and Samuelsen, Ø. (2019) OXA-48-Mediated ceftazidime-avibactam resistance is associated with evolutionary trade-offs. *mSphere* **4**, e00024-19
46. Hecker, S. J., Reddy, K. R., Totrov, M., Hirst, G. C., Lomovskaya, O., Griffith, D. C., et al. (2015) Discovery of a cyclic boronic acid  $\beta$ -lactamase inhibitor (RPX7009) with utility vs class A serine carbapenemases. *J. Med. Chem.* **58**, 3682–3692
47. Patel, T. S., Pogue, J. M., and Mills, J. P. (2018) Meropenem-vaborbactam: a new weapon in the war against infections due to resistant Gram-negative bacteria. *Future Microbiol.* **13**, 971–983
48. Lobstein, J., Emrich, C. A., Jeans, C., Faulkner, M., Riggs, P., and Berkmen, M. (2012) SHuffle, a novel *Escherichia coli* protein expression strain capable of correctly folding disulfide bonded proteins in its cytoplasm. *Microb. Cell Fact* **11**, 753
49. Ke, W., Bethel, C. R., Papp-Wallace, K. M., Pagadala, S. R. R., Nottingham, M., Fernandez, D., et al. (2012) Crystal structures of KPC-2  $\beta$ -lactamase in complex with 3-nitrophenyl boronic acid and the penam sulfone PSR-3-226. *Antimicrob. Agents Chemother.* **56**, 2713–2718
50. Krishnan, N. P., Nguyen, N. Q., Papp-Wallace, K. M., Bonomo, R. A., and van den Akker, F. (2015) Inhibition of *Klebsiella* beta-Lactamases (SHV-1 and KPC-2) by avibactam: a structural study. *PLoS One* **10**, e0136813
51. Sun, Z., Mehta, S. C., Adamski, C. J., Gibbs, R. A., and Palzkill, T. (2016) Deep sequencing of random mutant libraries reveals the active site of the narrow specificity CphA metallo- $\beta$ -lactamase is fragile to mutations. *Sci. Rep.* **6**, 33195
52. Sun, Z., Hu, L., Sankaran, B., Prasad, B. V. V., and Palzkill, T. (2018) Differential active site requirements for NDM-1  $\beta$ -lactamase hydrolysis of carbapenem versus penicillin and cephalosporin antibiotics. *Nat. Commun.* **9**, 4524
53. Battye, T. G. G., Kontogiannis, L., Johnson, O., Powell, H. R., and Leslie, A. G. W. (2011) iMOSFLM : a new graphical interface for diffraction-image processing with MOSFLM. *Acta Crystallogr. D Biol. Crystallogr.* **67**, 271–281
54. Winn, M. D., Ballard, C. C., Cowtan, K. D., Dodson, E. J., Emsley, P., Evans, P. R., et al. (2011) Overview of the CCP 4 suite and current developments. *Acta Crystallogr. D Biol. Crystallogr.* **67**, 235–242
55. Adams, P. D., Afonine, P. V., Bunkóczi, G., Chen, V. B., Davis, I. W., Echols, N., et al. (2010) Phenix : a comprehensive Python-based system for macromolecular structure solution. *Acta Crystallogr. D Biol. Crystallogr.* **66**, 213–221
56. Emsley, P., Lohkamp, B., Scott, W. G., and Cowtan, K. (2010) Features and development of coot. *Acta Crystallogr. D Biol. Crystallogr.* **66**, 486–501
57. Pettersen, E. F., Goddard, T. D., Huang, C. C., Couch, G. S., Greenblatt, D. M., Meng, E. C., et al. (2004) UCSF Chimera?A visualization system for exploratory research and analysis. *J. Comput. Chem.* **25**, 1605–1612
58. Ke, W., Bethel, C. R., Thomson, J. M., Bonomo, R. A., and Van Den Akker, F. (2007) Crystal structure of KPC-2: insights into carbapenemase activity in class A  $\beta$ -lactamases. *Biochemistry* **46**, 5732–5740
59. Fiser, A., Do, R. K. G., and Šali, A. (2000) Modeling of loops in protein structures. *Protein Sci.* **9**, 1753–1773